Tazieffite, $Pb_{20}Cd_2(As,Bi)_{22}S_{50}Cl_{10}$, a new chloro-sulfosalt from Mutnovsky volcano, Kamchatka Peninsula, Russian Federation

MICHAEL ZELENSKI,[1] ANNA GARAVELLI,[2] DANIELA PINTO,[2] FILIPPO VURRO,[2,*]
YVES MOËLO,[3] LUCA BINDI,[4] EMIL MAKOVICKY,[5] AND ELENA BONACCORSI[6]

[1]Institute of Experimental Mineralogy, Moscow district, 142432, Chernogolovka, Russia
[2]Dipartimento Geomineralogico, Università degli Studi di Bari, Via E. Orabona 4, I-70125 Bari, Italy
[3]Institut des Matériaux Jean Rouxel (IMN), Université de Nantes, CNRS, 2 rue de la Houssinière, BP 32229, F-44322 Nantes Cedex 3, France
[4]Museo di Storia Naturale, Sezione di Mineralogia, Università degli Studi di Firenze, Via G. La Pira 4, I-50121 Firenze, Italy
[5]Department of Geography and Geology, University of Copenhagen, Øster Voldgade 10, DK-1350 København K., Denmark
[6]Dipartimento di Scienze della Terra, Università degli Studi di Pisa, Via Santa Maria 53, I-56126 Pisa, Italy

ABSTRACT

Tazieffite, ideally $Pb_{20}Cd_2(As,Bi)_{22}S_{50}Cl_{10}$, is a new mineral from the high-temperature fumaroles of the Mutnovsky volcano, Kamchatka Peninsula, Russian Federation. It occurs as tiny, slender, needle-shaped crystals, up to 400 μm long and 10 μm across, generally forming fibrous aggregates. Tazieffite is closely associated with greenockite, galena, mutnovskite, kudriavite, and Cd-rich cannizzarite. Other minerals spatially associated are pyrite, anhydrite, and cristobalite. Tazieffite is silvery-gray in color, occasionally with a magenta tint when it forms aggregates of extremely fine needles. It has a black streak and metallic luster. In plane-polarized incident light, tazieffite is weakly bireflectant and weakly pleochroic from dark gray to a blue-gray. Between crossed polars, the mineral is weakly anisotropic, without characteristic rotation tints. Reflectance percentages measured in air (R_{min} and R_{max}) for a single grain are 33.9, 34.1 (471.1 nm), 32.8, 33.0 (548.3 nm), 32.4, 32.6 (586.6 nm), and 30.9, 31.1 (652.3 nm), respectively. Electron microprobe analyses yield the following ranges of concentrations: Pb 41.88–44.14 (avg. 42.90), Cd 0.87–1.16 (avg. 1.03), Sn 0.31–0.69 (avg. 0.48), Bi 20.43–22.94 (avg. 21.90), As 8.64–10.73 (avg. 9.66), S 16.10–17.48 (avg. 16.58), Se 0.82–1.28 (avg. 1.04), Cl 2.39–2.77 (avg. 2.63), Br 0.09–0.15 (avg. 0.12), I 0.27–0.58 (avg. 0.42). The empirical chemical formula, calculated on the basis of 44 cations, is $Pb_{20.06}(Cd_{0.89}Sn_{0.39}In_{0.02})_{\Sigma1.30}(As_{12.49}Bi_{10.15})_{\Sigma22.64}(S_{50.08}Se_{1.28})_{\Sigma51.36}(Cl_{7.18}I_{0.32}Br_{0.15})_{\Sigma7.65}$. Tazieffite is closely related to the halogen-sulfosalt vurroite, $Pb_{20}Sn_2Bi_{22}S_{54}Cl_6$, both from a chemical and structural point of view. It represents the (Cd,As)-dominant of vurroite, according to the coupled heterovalent substitution $Sn^{4+} + 2S^{2-} \rightarrow Cd^{2+} + 2Cl^-$. The crystal structure of tazieffite was refined in the space group $C2/c$ to $R = 0.0370$ for 4271 reflections with $I > 2\sigma(I)$. Unit-cell parameters are $a = 8.3520(17)$, $b = 45.5920(92)$, $c = 27.2610(55)$ Å, $\beta = 98.84(3)°$, with $V = 10257(4)$ Å^3, and $Z = 4$. The structure of tazieffite consists of lozenge-shaped composite rods made of coordination polyhedra of Pb around an octahedrally coordinated (Cd,Sn,Pb) position, interconnected into layers parallel to (010). These layers are separated by ribbons of As and Bi in distorted octahedral coordination. The ribbons form wavy, discontinuous double layers of the PbS archetype. Lone electron pairs of As and Bi are accommodated in the central portions of the PbS-like layers. The possibility that small amounts of NH_4^+ are incorporated in the crystal structure of tazieffite is discussed. The name of this new mineral species (IMA 2008-012) honors Haroun Tazieff (Warszawa, May 11, 1914–Paris, February 6, 1998), famous Belgian/French volcanologist, who was a pioneer in the field study of volcanoes and devoted his life to the study of volcanic gases.

Keywords: Tazieffite, chloro-sulfosalt, Mutnovsky volcano, fumaroles, vurroite isotype

INTRODUCTION

The fumarole system of Mutnovsky volcano (Kamchatka Peninsula, Russian Federation) is certainly an interesting and promising source of new and rare minerals. Not long after the find of the unusual iodine-bearing sulfosalt, mutnovskite [$Pb_2AsS_3(I,Cl,Br)$], at this site (Zelenski et al. 2006), another

new and interesting phase, tazieffite [$Pb_{20}Cd_2(As,Bi)_{22}S_{50}Cl_{10}$], has been discovered among sublimates collected from the area. Tazieffite is a complex sulfosalt containing Cl and Cd as essential chemical constituents together with major Pb, As, and Bi. After kudriavite, $(Cd,Pb)Bi_2S_4$ (Chaplygin et al. 2005), the new mineral represents the second sulfosalt containing Pb, Cd, and Bi found in nature, and the first having also As as an essential constituent. Tazieffite shows strong similarity with vurroite, $Pb_{20}Sn_2(Bi,As)_{22}S_{54}Cl_6$, recently discovered in high-temperature

fumarole deposits of Vulcano, Aeolian Islands, Italy (Pinto 2004; Garavelli et al. 2005).

The new mineral is named after Haroun Tazieff (Warszawa, May 11, 1914–Paris, February 6, 1998), famous Belgian, then French volcanologist who was a pioneer in the modern field study of active volcanoes, especially concerning the study of volcanic gases. The origin of the new mineral, which forms as a sublimate directly from volcanic fluids discharging from high-temperature fumaroles, inspired the name and makes tazieffite an appropriate memorial to Haroun Tazieff. The type material is housed in the mineralogical collection of the Museum "C.L. Garavelli," Dipartimento Geomineralogico, Università di Bari, under the catalog number 8/nm–V28. Additional samples are deposited in the mineralogical collections of both the Fersman Museum, Moscow (catalog number 92674), and the Ecole des Mines de Paris (catalog number 78986). Both the mineral and mineral name have been approved by the IMA Commission on New Minerals, Nomenclature and Classification (2008-012).

OCCURRENCE AND ASSOCIATED MINERALS

Tazieffite was found among volcanic sublimates of Mutnovsky volcano, Kamchatka Peninsula, Far East Asia, Russia (52.35° N, 158.27° E). It was deposited at a temperature ranging from 250 to 350 °C. For more details on the geological context and fumarole description, see Zelenski and Bortnikova (2005).

In hand specimens, tazieffite occurs as tiny, slender, needle-shaped crystals generally forming fibrous aggregates randomly accreted in holes and fissures of the volcanic rocks (Fig. 1). Needles are up to 400 µm long and 10 µm across. In the studied samples tazieffite is closely associated with greenockite, galena, mutnovskite, and two Cd-bearing Pb-Bi sulfosalts, kudriavite and Cd-rich cannizzarite. The paragenetic sequence of deposition observed in hand specimens collected from the ground suggests that tazieffite crystallized after greenockite, kudriavite, and Cd-rich cannizzarite, but before mutnovskite (Fig. 1). Other mineral phases spatially associated with tazieffite are pyrite, anhydrite, and cristobalite.

OPTICAL AND PHYSICAL PROPERTIES

Tazieffite is silver-gray in color, occasionally with a magenta tint when it forms aggregates of extremely fine needles. It has a black streak and a metallic luster. In plane-polarized incident light, tazieffite is weakly bireflectant and weakly pleochroic from dark gray to blue-gray. Between crossed polars, the mineral is weakly anisotropic, without distinct polarization colors.

The reflectance was measured in air with a MPM-200 Zeiss microphotometer equipped with a MSP-20 system processor on a Zeiss Axioplan ore microscope. Filament temperature was ~3350 K. Reflectance measurements were performed for specimen and standard (SiC) under the same focus conditions. The diameter of the measured area was 0.05 mm. Reflectance values (%) for R_{min} and R_{max} measured at the standard wavelengths (λ) 471.1, 548.3, 586.6, and 652.3 nm are reported in Table 1. Tazieffite appears to be slightly less reflective than vurroite.

Tazieffite crystals are brittle. No cleavage was observed. The density could not be measured owing to the small size of the crystals. The calculated density (from the empirical formula and single-crystal data) is 6.07 g/cm³.
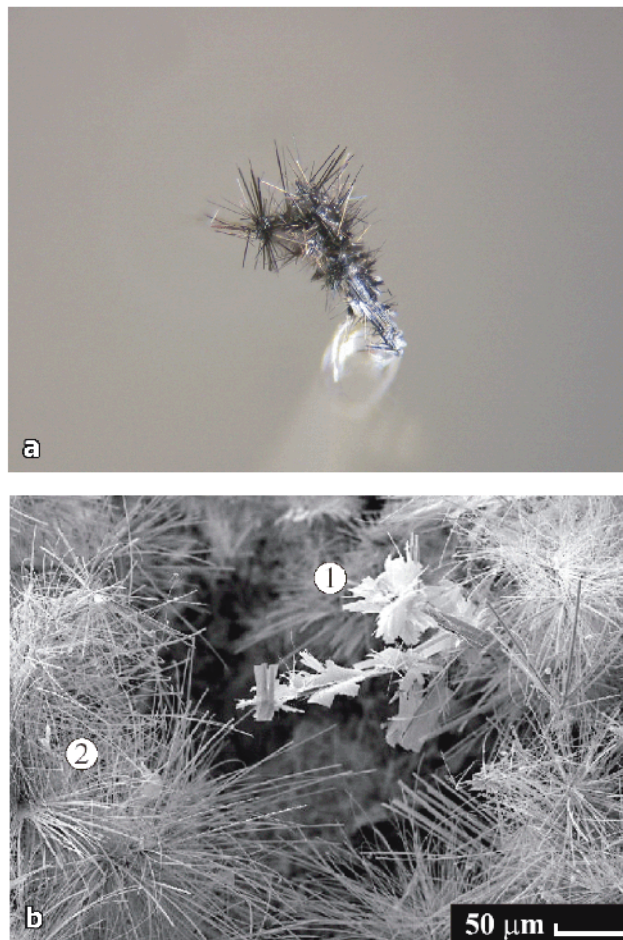
FIGURE 1. (**a**) Microphoto of fibrous aggregates of tazieffite (Photo by J.-M. Johannet). (**b**) Scanning electron photomicrograph of tazieffite crystals (BSE image); 1 = Cd-rich cannizzarite; 2 = tazieffite needle aggregates.

TABLE 1. Reflectance measurements in air for tazieffite

λ (nm)	R_{min} (%)	R_{max} (%)
471.1	33.9	34.1
548.3	32.8	33.0
586.6	32.4	32.6
652.3	30.9	31.1

CHEMICAL COMPOSITION

Two needle-like crystals of tazieffite were analyzed with a CAMECA SX 50 electron microprobe (BRGM-CNRS-University common laboratory, Orléans, France). The operating conditions were: accelerating voltage 20 kV, beam current 20 nA; standards (element, emission line, counting time for one spot analysis): FeS_2 (S$K\alpha$, 30 s), PbS (Pb$M\alpha$, 30 s), SnO_2 (Sn$L\alpha$, 20 s), Bi metal (Bi$M\alpha$, 30 s), AsGa (As$L\alpha$, 20 s), Cd metal (Cd$L\alpha$, 20 s), $TlAsS_2$ (Tl$M\alpha$, 10 s), elemental Se (Se$L\alpha$, 20 s), $Pb_5(VO_4)_3Cl$ (Cl$K\alpha$, 30 s), $MnSbS_2Br$ (Br$L\alpha$, 20 s), $Bi_{19}S_{18}I_3$ (I$L\alpha$, 10 s), and $CuInS_2$ (In$L\alpha$, 10 s). Fe, Mn, Cu, Zn, Ag, Sb, and Re were also included in the file, but not detected. Analytical results and average chemical composition (in wt% of elements) are reported in Table 2a. Low totals are due to the thickness of the analyzed fibers (<10 µm). Nevertheless, the valence balance is rather good:

TABLE 2a. Microprobe analysis of tazieffite: Chemical composition (wt%)

No.	Pb	Cd	Sn	Tl	In	Bi	As	S	Se	Cl	Br	I	Total*	Val % †
1	41.88	1.07	0.52	0.00	0.00	20.43	10.40	16.39	0.83	2.64	0.13	0.27	94.56	2.57
2	42.17	1.04	0.69	0.07	0.00	21.57	10.73	17.34	0.82	2.39	0.09	0.39	97.30	1.28
3	41.96	1.16	0.56	0.00	0.00	21.60	10.70	17.48	0.85	2.48	0.13	0.41	97.33	−0.31
4	42.52	1.01	0.31	0.00	0.00	21.95	9.28	16.10	1.23	2.67	0.15	0.40	95.62	0.87
5	43.54	1.03	0.39	0.00	0.00	22.14	8.64	16.25	1.11	2.68	0.09	0.58	96.45	−0.68
6	44.08	0.87	0.43	0.00	0.00	22.94	8.92	16.11	1.16	2.76	0.11	0.41	97.79	2.25
7	44.14	1.05	0.48	0.00	0.12	22.65	8.96	16.36	1.28	2.77	0.15	0.49	98.45	0.98
Average	42.90	1.03	0.48	0.01	0.02	21.90	9.66	16.58	1.04	2.63	0.12	0.42	96.79	0.94
Minimum	41.88	0.87	0.31	0.00	0.00	20.43	8.64	16.10	0.82	2.39	0.09	0.27		
Maximum	44.14	1.16	0.69	0.07	0.12	22.94	10.73	17.48	1.28	2.77	0.15	0.58		
St. dev.	1.00	0.09	0.12	0.03	0.05	0.82	0.91	0.58	0.20	0.14	0.03	0.10		

* Low totals due to the small thickness (<10 μm) of analyzed fibers.
† Relative error on the valence equilibrium (%), according to the formula: $[\Sigma(val^+) - \Sigma(val^-)] \times 100/\Sigma(val^-)$.

TABLE 2b. Microprobe analysis of tazieffite: Empirical formulae (basis: 44 cations)

1	$Pb_{19.65}(Cd_{0.93}Sn_{0.43})_{\Sigma1.36}(As_{13.49}Bi_{9.50})_{\Sigma23.00}(S_{49.70}Se_{1.02})_{\Sigma50.72}(Cl_{7.24}I_{0.21}Br_{0.16})_{\Sigma7.61}$
2	$Pb_{19.24}(Cd_{0.87}Sn_{0.55})_{\Sigma1.42}(As_{13.54}Bi_{9.76}Tl_{0.03})_{\Sigma23.30}(S_{51.14}Se_{0.98})_{\Sigma52.12}(Cl_{6.37}I_{0.29}Br_{0.11})_{\Sigma6.77}$
3	$Pb_{19.21}(Cd_{0.98}Sn_{0.45})_{\Sigma1.43}(As_{13.55}Bi_{9.81})_{\Sigma23.36}(S_{51.73}Se_{1.02})_{\Sigma52.75}(Cl_{6.64}I_{0.31}Br_{0.15})_{\Sigma7.10}$
4	$Pb_{20.26}(Cd_{0.89}Sn_{0.26})_{\Sigma1.15}(As_{12.23}Bi_{10.37})_{\Sigma22.60}(S_{49.58}Se_{1.54})_{\Sigma51.12}(Cl_{7.43}I_{0.31}Br_{0.19})_{\Sigma7.93}$
5	$Pb_{20.83}(Cd_{0.91}Sn_{0.33})_{\Sigma1.24}(As_{11.43}Bi_{10.50})_{\Sigma21.93}(S_{50.25}Se_{1.39})_{\Sigma51.64}(Cl_{7.49}I_{0.45}Br_{0.11})_{\Sigma8.05}$
6	$Pb_{20.67}(Cd_{0.75}Sn_{35})_{\Sigma1.10}(As_{11.57}Bi_{10.66})_{\Sigma22.23}(S_{48.81}Se_{1.43})_{\Sigma50.24}(Cl_{7.56}I_{0.31}Br_{0.13})_{\Sigma8.00}$
7	$Pb_{20.58}(Cd_{0.90}Sn_{0.39}In_{0.10})_{\Sigma1.39}(As_{11.55}Bi_{10.47})_{\Sigma22.02}(S_{49.30}Se_{1.57})_{\Sigma50.87}(Cl_{7.55}I_{0.37}Br_{0.18})_{\Sigma8.10}$
Avg.	$Pb_{20.06}(Cd_{0.89}Sn_{0.39}In_{0.02})_{\Sigma1.30}(As_{12.49}Bi_{10.15})_{\Sigma22.64}(S_{50.08}Se_{1.28})_{\Sigma51.36}(Cl_{7.18}I_{0.32}Br_{0.15})_{\Sigma7.65}$

deviations do not exceed about 2.6% in absolute value.

Tazieffite contains significant amounts of Cd [up to 0.98 atoms per formula unit (apfu)] and Sn (up to 0.55 apfu) in addition to the major cations Pb (19.21–20.83 apfu), Bi (9.50–10.66 apfu), and As (11.43–13.55 apfu), as well as minor concentrations of Br (up to 0.19 apfu), I (up to 0.45 apfu), Se (up to 1.57 apfu), in addition to the major anions S (48.81–51.73 apfu) and Cl (6.37–7.56 apfu). Traces of Tl and In were detected occasionally. Table 2b reports several empirical chemical formulae of tazieffite calculated on the basis of 44 cations per formula unit, as indicated by the structural data (see below). The resulting average empirical formula for tazieffite is: $Pb_{20.06}(Cd_{0.89}Sn_{0.39}In_{0.02})_{\Sigma1.30}$ $(As_{12.49}Bi_{10.15})_{\Sigma22.64}(S_{50.08}Se_{1.28})_{\Sigma51.36}(Cl_{7.18}I_{0.32}Br_{0.15})_{\Sigma7.65}$.

Taking into account the results derived from the refinement of the occupancy factors, the chemical formula can be written as $(Pb_{19.36}Bi_{0.64})_{\Sigma20.00}(Cd_{0.89}Pb_{0.70}Sn_{0.39}In_{0.02})_{\Sigma2.00}(As_{12.49}Bi_{9.51})_{\Sigma22.00}$ $(S_{50.08}Se_{1.28})_{\Sigma51.36}(Cl_{7.18}I_{0.32}Br_{0.15})_{\Sigma7.65}$, which can be simplified as the ideal end-member formula $Pb_{20}Cd_2(As,Bi)_{22}S_{50}Cl_{10}$ (see below, the paragraph "relationship to vurroite").

X-RAY DIFFRACTION STUDY

X-ray powder diffraction

The X-ray powder diffraction pattern for the holotype (Table 3) was obtained using a 57.3 mm diameter Debye-Scherrer camera (Fe$K\alpha$). Indexing of the reflections was done on the basis of the calculated powder pattern obtained with the structural model presented below. The unit-cell parameters obtained by the least-squares refinement of 52 reflections are: $a = 8.337(9)$, $b = 45.67(2)$, $c = 27.23(2)$ Å, $\beta = 98.8(1)°$, and $V = 10246(23)$ Å^3.

Single-crystal X-ray diffraction

A preliminary X-ray study was performed on a selected needle-like crystal of tazieffite using a Bruker-AXS SMART-APEX II diffractometer equipped with a CCD detector and

Mo$K\alpha$ monochromatized radiation ($\lambda = 0.71073$ Å; operating conditions: 50 kV and 35 mA). The orthorhombic primitive unit cell obtained was very close to the sub-cell of vurroite (i.e., "family structure," space group $Pmmn$, lattice parameters $a \approx 22.8$, $b \approx 4.2$, $c \approx 27.3$ Å), suggesting that the crystal structure of tazieffite could belong to the same OD-family as that of vurroite (Pinto et al. 2008).

To check for the presence of weaker superstructure reflections, a new intensity data collection was then performed on the same crystal at the Elettra synchrotron facility (Basovizza–Trieste, Italy). The wavelength of the radiation was set to 1.0 Å, and the crystal was placed at 40 mm from the 165 mm MarCCD detector. Ninety frames were collected with a rotation angle $\Delta\varphi = 2°$. The collected frames included some strong maxima for $h = 2n$ in addition to weak reflections for $h = 2n + 1$ of a monoclinic unit cell, space group symmetry $C2/c$, and lattice parameters $a = 8.3520(17)$, $b = 45.5920(92)$, $c = 27.2610(55)$ Å, $\beta = 98.84(3)°$, thus showing a reciprocal lattice very close to that of vurroite (Pinto et al. 2008). As a matter of fact, reflections with even h correspond to the family reflections of the vurroite OD-family, whereas those with odd h correspond to reflections characteristic of the ordered polytype MDO1 of this family. For a comprehensive description of the OD-character of vurroite, the OD-groupoid symbol, and MDO polytypes, see Pinto et al. (2008). No characteristic reflections of the polytype MDO2 could be found in the investigated crystal, or in several different crystals of tazieffite from the same locality measured at the Elettra facility. Indeed, for most of the crystals examined, the X-ray pattern showed only diffuse streaks parallel to **b*** for $h = 2n + 1$ in addition to sharp and strong maxima for even h (family reflections), suggesting a prevalence of completely disordered crystals among tazieffite samples from Mutnovsky.

Details about the data collection and refinement are summarized in Table 4. Reduction of the data, including intensity integration, background and Lorenz-polarization corrections, was done using the HKL package of programs (XDISP, DENZO, and SCALEPACK; Otwinowsky and Minor 1997).

The crystal structure refinement was initially carried out with the program SHELXL-97 (Sheldrick 1997) starting from the atomic coordinates reported by Pinto et al. (2008) for the crystal structure of vurroite. The refinement ($R \approx 13\%$) evidenced anomalous environments for some of the Pb and Bi structural sites and some large residuals (up to ≈ 5 e$^-$/Å^3, close to S1 and S2 positions) in the difference Fourier syntheses. The intensity data set was then treated using the JANA2000 program suite

TABLE 3. X-ray powder-diffraction data for tazieffite

h	k	l	d_{calc} (Å)	I/I_o	d_{obs} (Å)	I/I_o
0	2	1	17.4012	6.81	–	–
0	4	0	11.3980	0.86	11.40	3
0	4	2	8.7006	7.06	8.69	7
0	6	1	7.3133	11.63	7.32	12
0	6	2	6.6181	2.15	6.62	5
1	5	1	5.8252	3.01	s5.82	4
0	8	2	5.2485	4.74	5.26	8
$\bar{1}$	4	4	5.0702	2.18	5.07	5
0	0	6	4.4895	8.77	4.48	9
0	8	4	4.3503	23.61	4.35	21
0	4	6	4.1772	4.91	4.17	8
$\bar{2}$	0	2	4.1270	4.10		
$\bar{2}$	2	1	4.1076	15.12	4.07	39
0	10	3	4.0652	33.19		
$\bar{2}$	4	1	3.9211	11.88	3.90	3
0	8	5	3.9150	3.74		
0	6	6	3.8653	11.30		
0	12	0	3.7993	8.65	3.80	53
0	2	7	3.7945	14.14		
0	12	2	3.6566	32.11	3.66	24
0	4	7	3.6460	6.56		
$\bar{2}$	6	2	3.6266	7.90		
2	6	0	3.6262	9.29		
$\bar{2}$	4	4	3.5940	15.87	3.58	7
2	4	2	3.5928	16.44		
$\bar{2}$	6	3	3.5321	27.52	3.52	14
2	6	1	3.5313	27.20		
0	8	6	3.5267	3.74		
$\bar{2}$	2	5	3.5075	8.32		
2	2	3	3.5060	8.16		
0	10	5	3.4802	15.23	3.48	17
$\bar{2}$	8	1	3.3685	6.62	3.361	65
0	0	8	3.3671	72.67		
$\bar{2}$	8	2	3.3426	8.91		
2	8	0	3.3423	10.73		
0	12	4	3.3090	100.00	3.313	100
$\bar{2}$	6	5	3.2162	16.00	3.215	6
2	6	3	3.2150	12.54		
0	8	7	3.1892	4.26	3.169	6
$\bar{2}$	4	6	3.1710	17.73		
2	4	4	3.1696	18.02		
$\bar{2}$	8	4	3.1543	12.91		
2	8	2	3.1534	13.96		
$\bar{2}$	10	1	3.0795	4.94	–	–
$\bar{2}$	2	7	3.0313	3.97	–	–
2	2	5	3.0298	4.58	3.001	3
0	12	6	2.9002	13.25	2.900	12
$\bar{2}$	8	6	2.8567	16.49	2.835	39
2	8	4	2.8556	15.34		
$\bar{2}$	6	7	2.8373	45.71		
2	6	5	2.8361	43.67		
$\bar{2}$	0	8	2.8306	20.54		
2	0	6	2.8292	20.83		
$\bar{2}$	10	5	2.8009	15.81	2.789	36
2	10	3	2.8002	16.09		
$\bar{2}$	12	2	2.7952	3.02		
2	12	0	2.7950	4.83		
0	14	5	2.7870	26.72		
$\bar{2}$	4	8	2.7471	9.13	2.745	5
2	4	6	2.7459	11.58		
$\bar{2}$	12	4	2.6822	4.00	2.683	6
$\bar{2}$	14	1	2.5680	13.00	2.569	4
$\bar{2}$	10	7	2.5399	5.87	2.527	14
2	10	5	2.5390	7.01		
$\bar{2}$	8	8	2.5351	6.77		
2	8	6	2.5341	6.72		
$\bar{2}$	14	3	2.5227	10.16		
2	14	1	2.5224	9.41		
0	18	1	2.5218	7.96		
0	1	11	2.4453	3.65	2.441	5
0	20	0	2.2796	4.93	2.280	6
$\bar{2}$	12	8	2.2699	5.56		
2	12	6	2.2692	4.13		
$\bar{2}$	8	10	2.2378	10.27	2.231	8

TABLE 3.—_Continued_

h	k	l	d_{calc} (Å)	I/I_o	d_{obs} (Å)	I/I_o
2	8	8	2.2370	10.13		
0	12	10	2.1975	10.37	2.191	8
0	16	8	2.1751	5.81		
$\bar{2}$	6	11	2.1699	12.66	2.168	4
2	6	9	2.1690	11.88		
$\bar{2}$	18	1	2.1657	27.50		
$\bar{2}$	18	2	2.1587	3.46	2.152	9
2	18	0	2.1587	3.51		
0	10	11	2.1573	15.46		
$\bar{2}$	18	3	2.1383	5.45	–	–
2	18	1	2.1381	6.10	–	–
0	18	7	2.1157	4.41	–	–
0	8	12	2.0886	3.11	2.087	6
$\bar{4}$	0	2	2.0880	57.11		
$\bar{2}$	4	12	2.0775	6.95	–	–
2	4	10	2.0766	7.01	–	–
0	2	13	2.0636	3.92	2.068	6
$\bar{2}$	12	10	2.0491	4.96	2.047	4
2	12	8	2.0484	6.12		
0	18	8	2.0241	3.21	2.023	5
$\bar{2}$	20	2	1.9954	6.47	–	–
2	20	0	1.9954	5.33	–	–
$\bar{2}$	8	12	1.9811	9.60	1.979	4
2	8	10	1.9804	10.39		
$\bar{4}$	8	2	1.9606	1.25	1.960	2
$\bar{2}$	20	4	1.9531	4.34	–	–
2	20	2	1.9529	4.26	–	–
0	12	12	1.9326	17.99	1.930	6
$\bar{2}$	6	13	1.9139	4.19	1.906	5
2	6	11	1.9131	3.91		
0	24	0	1.8997	6.87	1.887	3
$\bar{2}$	20	6	1.8758	5.04	–	–
2	20	4	1.8756	5.12	–	–
$\bar{4}$	10	5	1.8575	3.09	1.858	2
4	10	1	1.8572	4.68		
$\bar{2}$	4	14	1.8324	5.75	1.833	3
2	4	12	1.8317	5.75		
$\bar{2}$	18	9	1.8217	11.92	1.823	5
2	18	7	1.8212	12.22		
$\bar{4}$	12	4	1.8133	4.09	–	–
4	12	0	1.8131	4.13	–	–
$\bar{4}$	0	10	1.7749	12.47	–	–
4	0	6	1.7741	10.69	–	–
$\bar{4}$	12	6	1.7660	15.19	1.761	4
4	12	2	1.7656	15.35		
0	16	12	1.7633	3.10		
0	24	6	1.7495	6.39	1.753	4
0	26	3	1.7210	3.32	1.726	3
0	0	16	1.6836	10.94	1.698	3
0	18	12	1.6800	3.14	1.680	5
$\bar{4}$	14	7	1.6712	4.03	–	–
4	14	3	1.6708	4.51		
0	26	5	1.6674	4.46	–	–
0	24	8	1.6545	5.70	–	–
$\bar{4}$	12	12	1.5140	3.25	–	–
$\bar{4}$	10	13	1.5007	4.38	–	–
4	10	9	1.5000	3.96	–	–
$\bar{4}$	12	14	1.4186	5.76	–	–
4	12	10	1.4180	5.27	–	–
$\bar{4}$	24	2	1.4051	4.71	–	–
$\bar{2}$	30	5	1.3971	3.81	–	–
2	30	3	1.3970	3.91	–	–
$\bar{2}$	12	18	1.3805	3.12	–	–
2	12	16	1.3801	3.32	–	–
$\bar{2}$	18	17	1.3293	5.42	–	–
2	18	15	1.3290	5.17	–	–
$\bar{4}$	0	18	1.3109	4.10	–	–

Note: (1) d_{calc} = calculated powder pattern and indexing for tazieffite. d values calculated on the basis of a = 8.3520(17) Å, b = 45.592(9) Å, c = 27.2610(6) Å, β = 98.84(3)°, and with the atomic coordinates and site occupancies reported in Table 5. Intensities calculated using XPOW software version 2.0 (Downs et al. 1993). (2) d_{obs} = observed powder pattern obtained with a 57.3 mm diameter Debye-Scherrer camera (Fe$K\alpha$).

TABLE 4. Crystal data and summary of parameters describing data collection and refinement for tazieffite

|	
Crystal data	
X-ray formula	$Pb_{20.26}(NH_4)_{0.24}Cd_{1.00}Sn_{0.50}As_{12.82}Bi_{9.18}S_{52}Cl_8$
Crystal size (mm)	$0.006 \times 0.010 \times 0.300$
Cell setting, space group	Monoclinic, $C2/c$
a, b, c (Å); β (°)	8.3520(17), 45.592(9), 27.261(6) Å; 98.84(3)°
V (Å^3)	10257(4)
Z	4
Dx (g/cm^3)	6.077
Data collection	
Radiation, λ (Å)	synchrotron, 1.00
Temperature (K)	293
Detector to sample distance (mm)	40
Active detection-area (cm^2)	16.5×16.5
Number of frames	90
Rotation width per frame (°)	2
Measuring time (s)	dose = 150
Maximum observed 2θ	65.08 ($d = 0.88$ Å)
Unique reflections	5748
Reflections $F_o > 4\sigma F_o$	4271
R_{int} after absorption correction	0.0513
R_σ	0.0979
Range of h, k, l	$-7 \leq h \leq 8, -48 \leq k \leq 48, -24 \leq l \leq 29$
Refinement	
$R [F_o > 4\sigma (F_o)]$	0.0370
R (all data)	0.0689
wR (on F_o^2)	0.0851
wR (all data)	0.0847
Goof	0.851
Number of least squares parameters	319

(Petříček et al. 2000). JANA2000 adopts a different strategy than does the SHELX package in the merging of symmetry-equivalent reflections. For details of the averaging of equivalent reflections for twins in JANA2000, see the detailed description given in the appendix in Gaudin et al. (2000). The subsequent refinement carried out with JANA2000 (again starting from the atomic coordinates reported by Pinto et al. 2008) showed more regular environments for the structural sites and a resulting structural formula in keeping with the microprobe data ($R \approx$ 7%). For the assignment of atomic species in the structure, interatomic distances and heights of maxima in Fourier maps were considered. Two of the Pb sites, M9 and M10, showed higher atomic displacement parameters and longer Pb-S distances than the other Pb positions in the structure. Refinements with free occupancy factors showed electron densities suggesting either a partial occupancy for these cation sites or the presence of a lighter cation partly substituting for Pb atoms. The presence of K or Ba was considered, but excluded since chemical scanning with electron microprobe did not show the presence of these large cations. The abundance of NH$_4$-bearing compounds in the fumarole system of Mutnovsky (Zelenski and Bortnikova 2005) suggested the possibility of NH$_4^+$ substituting for Pb in both M9 and M10 (see the crystal-chemical discussion below). Then, the structure refinement was carried out by refining Pb vs. Na for M9 and M10 sites. We choose Na as the atomic species because it has an electron number (i.e., 11) identical to that of the NH$_4$ group. According to this final model, we calculated 0.06 NH$_4^+$ in each position, leading to a total of 0.24 apfu of NH$_4$ (for the structure formula with 44 cations), which corresponds to an N content close to 0.037 wt%. Due to the extremely low N content, which lies below the detection limit of EPMA in ordinary analytical conditions, the presence of NH$_4$ in the structure of

tazieffite could not be supported by any microprobe data. Despite that, the occurrence of NH$_4^+$ together with Pb in M9 and M10 is considered as the most reasonable explanation for the observed coordination environment of these sites.

According to structural and crystal-chemical evidence, Cd has been assigned into the structure sites M12 and M13 (Fig. 2) in addition to minor amounts of Pb and Sn. Since Sn and Cd have similar scattering power, in the first step the sum Sn+Cd has been refined against Pb. This gave 0.2 Pb in M12 and 0.3 Pb in M13. Then the occupancy of Cd and Sn in each site (0.5 Cd and 0.3 Sn in M12; 0.5 Cd and 0.2 Sn in M13) has been assigned taking into account microprobe data.

Inspection of the F_{obs}-F_{calc} list revealed a quasi-systematic positive difference for the hkl reflections having $h = 2n$ (family reflections). As already observed in the structure of vurroite (Pinto et al. 2008), this is related to the presence in the crystal of a considerable percentage of fully disordered domains, admixed with the domains of the ordered MDO1 polytype. A second scale factor was then introduced for this kind of reflection [with a refined value of 0.617(3)] to eliminate the contribution of the disordered portions (Nespolo and Ferraris 2001; Pinto et al. 2008). This significantly improved the R value, which reached $R = 3.70\%$. Unlike vurroite, the application of separate scale factors for the family and the characteristic reflections did not allow the assignment of either pure Bi or As into the positions M14-M23 of the tazieffite structure, all of which, except M15, were finally refined with a mixed (As,Bi) occupancy. M17, M18, M20, and M22 were refined with isotropic and identical displacement parameters and the sum of occupancies was constrained to one, but the coordinates of Bi and As were kept independent. For all the other mixed (As,Bi) sites, both anisotropic displacement parameters and atom coordinates were constrained to be identical and the occupancies were constrained to 1.

Owing to the negligible difference in the scattering powers of S and Cl, bond-valence calculations were used for the identification of Cl among the anion sites. This allowed identifying five sites that are at least preferentially occupied by Cl. Two of them (Cl29 and Cl30) that showed bond-valence values close to one
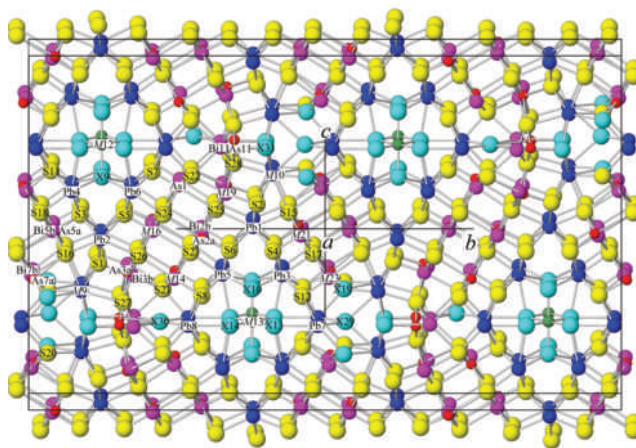
FIGURE 2. The crystal structure of tazieffite projected down [100]. Yellow = S atoms; light blue = Cl atoms; pink = Bi atoms; blue = Pb atoms and Pb-dominated sites; red = As atoms; green = (Cd,Pb,Sn) sites.

were assumed as full Cl sites, whereas X9, X10, X13, and X14 were considered as Cl-dominated (with about 60% Cl in each site). Finally, X19 and X31 were assumed as mixed $S_{0.70}Cl_{0.30}$ sites. However, as the M23 site does not have independent coordinates for As and Bi atoms, it is possible that the observed deficit of bond valence on the X19 site might be the result of the M23 site being slightly displaced with respect to a normal As coordination position. This would result in a lower bond valence of the ligand; therefore it is possible that the Cl content of X19 resulting from bond valence calculations is not correct. For all S and Cl atoms, anisotropic displacement parameters were used in the refinement.

As already observed in vurroite, also in the structure of tazieffite the anion position Cl29 does not show its counterpart at the $x = 0$ level. As a consequence, a very large cavity corresponding to the polyhedron built up by 2 Pb7, 2 Pb9, 2 X19, 2 S20, 2 X29, and 2 X31 is present (Fig. 3). This suggested the possible occurrence in this large cavity of a light ion or molecule (for instance HF or H_2O). Nevertheless, no concrete evidence of the presence of such a light chemical component in this position could be found from the list of the Fourier residues, indicating that if such a light component is actually present, its site occupancy is probably too low to be revealed in the Fourier map of tazieffite.

Fractional atomic coordinates, occupation factors, and displacement parameters of tazieffite structure are shown in Table 5. Table 6[1] lists the observed and calculated structure factors, whereas selected bond distances are shown in Table 7. Coordination parameters for cations are summarized in Table 8.

Description of the structure

The crystal structure of tazieffite strongly resembles that of vurroite (Garavelli et al. 2005; Pinto et al. 2008). The main features of the two structures are the same, with the same type of coordination, but with some geometrical differences, owing to the different chemistry and site populations. The structure of tazieffite contains lozenge-shaped composite rods made of coordination polyhedra of Pb around an octahedrally coordinated (Cd,Sn,Pb) position, interconnected into layers parallel to (010) of the standard monoclinic setting $C2/c$. These layers are separated by ribbons of coordination pyramids of As and Bi
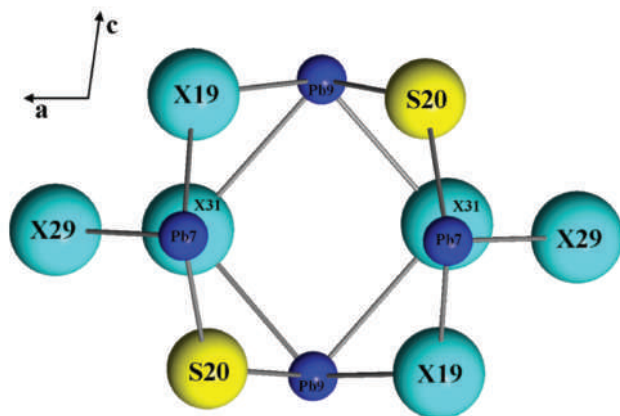

FIGURE 3. Large cavity corresponding to the polyhedron built up by 2 Pb7, 2 Pb9, 2 X19, 2 S20, 2 X29, and 2 X31. Colors as in Figure 2.

with the vertices of the pyramids oriented toward the rods (Fig. 4). The ribbons form wavy, discontinuous double layers of the PbS archetype (with As and Bi as cations), which are completed by rods of the trigonal prisms of M7, M8, and M11 at ¼ and ¾ z levels (the so-called "constricted layer portion" in the structure of vurroite). The PbS-like portions on the opposing sides of the lozenges are two and three pyramids wide, respectively (C and D rods, respectively; Fig. 4). Lone electron pairs of As and Bi are accommodated in the central portions of the PbS-like layers.

All Pb-dominated sites of the structure show trigonal prismatic coordination, with bases of the prisms normal to [100] in the case of M1-M6 and M9-M10 sites (standing trigonal prisms), and parallel to [100] for Pb7-Pb8 (lying-down trigonal prisms). The trigonal prisms of M1-M8, which form the main building element of the lozenge-shaped rods (Fig. 4), are characterized by cation-to-anion distances (Table 7) ranging from 2.874 to 3.404 Å and averaging about 3.06–3.10 Å. Unlike the results obtained for vurroite, no evidence suggesting an incorporation of Bi (or additional cations) in these structure positions of tazieffite can be observed; in vurroite, M7 and M8 showed about 20 and 40% of Bi substituting for Pb, respectively. The bond valences calculated according to Brese and O'Keeffe (1991) range from 1.96 to 2.06 (Table 8), thus indicating a pure Pb occupancy in M1-M8. The same conclusion is reached by comparing some coordination parameters such as the volume eccentricities (ECCv), the volume sphericities (SPHv) and the polyhedral volumes (Vp) calculated for the polyhedra around these sites (Table 8).

A comparison among selected bond distances (Table 7) clearly shows anomalous large coordination environments for both M9 and M10, with M-(S,Cl) distances ranging from 2.981 to 3.598 Å and averaging 3.18 and 3.27 Å, respectively (Table 8). Moreover, bond valences were significantly lower than the expected value for a fully occupied Pb site (~1.55 and ~1.40 for M9 and M10, respectively). As explained above, this feature suggested the presence of NH_4^+ substituting for Pb in both M9 and M10. A comparison between the coordination of these Pb-cation sites of tazieffite and that of NH_4^+ in the structure of NH_4CdCl_3 (Rolies and de Ranter 1978) provides support for this hypothesis. As a matter of fact, NH_4^+ is linked to 9 Cl atoms, thus showing a tricapped trigonal prismatic coordination, very similar to that of M10, but with a larger size. Selected N-Cl distances for NH_4CdCl_3 are (Å): 3.278 (×2), 3.316 (×2), 3.348 (×2), 3.433, 3.489, 3.818 (Rolies and de Ranter 1978). Since NH_4^+ has almost the same size as Tl^+ bond valences in Table 8 were calculated considering NH_4^+ as Tl^+, and then using the known Tl^+ parameter (Brese and O'Keeffe 1991). A clear evidence that bond-valence calculations for the ammonium cation can be performed to a good approximation by replacing the N atom with a Tl one is given by the comparison of the two isotypic minerals salt ammoniac,

---

[1] Deposit item AM-09-042, Table 6 (observed and calculated structure factors) and CIF. Deposit items are available two ways: For a paper copy contact the Business Office of the Mineralogical Society of America (see inside front cover of recent issue) for price information. For an electronic copy visit the MSA web site at http://www.minsocam.org, go to the American Mineralogist Contents, find the table of contents for the specific volume/issue wanted, and then click on the deposit link there.

TABLE 5. Fractional atomic coordinates, anisotropic displacement parameters, and occupancies for the crystal structure of tazieffite

Site	Atom	x	y	z	s.o.f.	U_{11}	U_{22}	U_{33}	U_{23}	U_{13}	U_{12}	U_{eq}
M1	Pb1	0.38646(21)	0.12162(1)	0.51217(3)	1	0.04749(62)	0.0488(4)	0.0572(5)	0.00023(28)	0.0083(11)	0.00069(69)	0.05115(24)
M2	Pb2	0.8868(2)	0.12146(1)	0.51230(3)	1	0.04614(59)	0.04637(38)	0.0547(5)	0.00030(27)	0.0075(11)	0.00092(67)	0.04908(23)
M3	Pb3	0.31117(22)	0.07257(1)	0.37217(3)	1	0.04770(56)	0.04788(39)	0.05684(45)	−0.0005(3)	0.0106(11)	0.00032(79)	0.05053(21)
M4	Pb4	0.81076(22)	0.07236(2)	0.37239(3)	1	0.04874(57)	0.0485(4)	0.05700(45)	−0.00012(31)	0.0106(11)	0.0003(8)	0.05117(21)
M5	Pb5	0.31093(21)	0.17319(2)	0.37403(3)	1	0.04664(53)	0.0469(4)	0.05657(45)	−0.0005(3)	0.0077(10)	−0.00001(81)	0.05006(21)
M6	Pb6	0.80952(21)	0.17349(2)	0.37463(3)	1	0.05015(74)	0.05042(41)	0.05978(47)	−0.00028(33)	0.0077(11)	0.00018(86)	0.05353(22)
M7	Pb7	0.7462(1)	0.98784(1)	0.74961(3)	1	0.04893(59)	0.04915(34)	0.05766(41)	−0.00007(32)	0.0078(14)	0.00035(37)	0.05196(20)
M8	Pb8	0.74433(11)	0.23103(2)	0.24995(3)	1	0.05955(69)	0.0612(4)	0.0695(5)	−0.00015(38)	0.0080(15)	−0.0003(4)	0.06360(24)
M9	Pb9	0.96003(22)	0.08875(2)	0.66171(3)	0.94(1)	0.05525(68)	0.05671(49)	0.0655(6)	0.00070(36)	0.0089(12)	0.00076(94)	0.05919(34)
	(NH₄)9	0.96003(22)	0.08875(2)	0.66171(3)	0.06(1)	0.05525(68)	0.05671(49)	0.0655(6)	0.00070(36)	0.0089(12)	0.00076(94)	0.05919(34)
M10	Pb10	0.45838(22)	0.08941(2)	0.66388(3)	0.94(1)	0.05731(66)	0.0585(5)	0.0671(6)	−0.00022(37)	0.0082(12)	0.00025(97)	0.06112(34)
	(NH₄)10	0.45838(22)	0.08941(2)	0.66388(3)	0.06(1)	0.05731(66)	0.0585(5)	0.0671(6)	−0.00022(37)	0.0082(12)	0.00025(97)	0.06112(34)
M11	Bi11	0.2413(3)	0.17680(4)	0.74583(8)	0.33(1)	0.0492(12)	0.04725(72)	0.05673(99)	0.00108(96)	0.0087(24)	0.00115(98)	0.05100(46)
	As11	0.24526(38)	0.15307(6)	0.75122(12)	0.67(1)	0.0492(12)	0.04725(72)	0.05673(99)	0.00108(96)	0.0087(24)	0.00115(98)	0.05100(46)
M12	Cd1a	0	0.12313(3)	0.25	0.5	0.0531(13)	0.0572(9)	0.0654(11)	0.00000	0.0091(25)	0.00000	0.05858(46)
	Pb1b	0	0.12313(3)	0.25	0.2	0.0531(13)	0.0572(9)	0.0654(11)	0.00000	0.0091(25)	0.00000	0.05858(46)
	Sn1c	0	0.12313(3)	0.25	0.3	0.0531(13)	0.0572(9)	0.0654(11)	0.00000	0.0091(25)	0.00000	0.05858(46)
M13	Cd2a	0.5	0.12322(3)	0.25	0.5	0.0546(12)	0.05526(83)	0.0627(10)	0.00000	0.0094(23)	0.00000	0.05747(42)
	Pb2b	0.5	0.12322(3)	0.25	0.3	0.0546(12)	0.05526(83)	0.0627(10)	0.00000	0.0094(23)	0.00000	0.05747(42)
	Sn2c	0.5	0.12322(3)	0.25	0.2	0.0546(12)	0.05526(83)	0.0627(10)	0.00000	0.0094(23)	0.00000	0.05747(42)
M14	Bi1a	0.56454(29)	0.25498(3)	0.37431(3)	0.71(1)	0.0487(7)	0.04884(51)	0.05880(58)	0.00018(38)	0.0077(13)	−0.0001(9)	0.05216(35)
	As1b	0.56454(29)	0.25498(3)	0.37431(3)	0.29(1)	0.0487(7)	0.04884(51)	0.05880(58)	0.00018(38)	0.0077(13)	−0.0001(9)	0.05216(35)
M15	As1	0.43461(76)	0.24664(8)	0.62661(9)	1	0.0662(20)	0.0634(15)	0.0797(16)	0.0016(11)	0.0090(37)	0.0010(26)	0.06996(72)
M16	Bi2a	0.12308(25)	0.20938(2)	0.49898(4)	0.69(1)	0.05526(77)	0.05570(63)	0.06461(73)	0.00089(44)	0.0073(10)	0.00035(64)	0.05872(43)
	As2b	0.12308(25)	0.20938(2)	0.49898(4)	0.31(1)	0.05526(77)	0.05570(63)	0.06461(73)	0.00089(44)	0.0073(10)	0.00035(64)	0.05872(43)
M17	As2a	0.6236(18)	0.20835(17)	0.49001(28)	0.63(1)	0.06399(82)						
	Bi2b	0.6172(11)	0.20835(12)	0.49773(16)	0.37(1)	0.06399(82)						
M18	As3a	0.1905(11)	0.1660(1)	0.61939(14)	0.79(1)	0.05898(80)						
	Bi3b	0.1912(14)	0.17298(12)	0.62680(19)	0.21(1)	0.05898(80)						
M19	Bi4a	0.67961(28)	0.16706(3)	0.61994(3)	0.62(1)	0.04805(68)	0.04757(52)	0.05617(60)	−0.00083(38)	0.00861(75)	0.00168(83)	0.05053(36)
	As4b	0.67961(28)	0.16706(3)	0.61994(3)	0.38(1)	0.04805(68)	0.04757(52)	0.05617(60)	−0.00083(38)	0.00861(75)	0.00168(83)	0.05053(36)
M20	As5a	0.12372	0.0450(1)	0.50404(22)	0.69(1)	0.06210(79)						
	Bi5b	0.1210(14)	0.0398(1)	0.49889(17)	0.31(1)	0.06210(79)						
M21	Bi6a	0.62272(29)	0.04079(2)	0.49918(4)	0.57(1)	0.05862(88)	0.05731(70)	0.06686(84)	−0.00092(50)	0.0126(11)	0.0020(11)	0.06062(48)
	As6b	0.62272(29)	0.04079(2)	0.49918(4)	0.43(1)	0.05862(88)	0.05731(70)	0.06686(84)	−0.00092(50)	0.0126(11)	0.0020(11)	0.06062(48)
M22	As7a	0.9346(11)	0.00891(8)	0.62961(15)	0.83(1)	0.0601(9)						
	Bi7b	0.9357(21)	0.00445(14)	0.61602(27)	0.17(1)	0.0601(9)						
M23	Bi8a	0.43260(34)	0.00658(3)	0.62309(4)	0.61(1)	0.05838(87)	0.05853(69)	0.06794(73)	−0.00051(47)	0.0103(15)	0.00008(84)	0.06155(41)
	As8b	0.43260(34)	0.00658(3)	0.62309(4)	0.39(1)	0.05838(87)	0.05853(69)	0.06794(73)	−0.00051(47)	0.0103(15)	0.00008(84)	0.06155(41)
X1	S1	0.1574(16)	0.11787(12)	0.59346(22)	1	0.0707(50)	0.0753(31)	0.0750(35)	−0.0038(26)	0.0153(57)	−0.0063(51)	0.0732(18)
X2	S2	0.6610(17)	0.11471(12)	0.58893(21)	1	0.0697(44)	0.0750(33)	0.0800(35)	−0.0048(26)	0.0125(58)	−0.0046(53)	0.0748(16)
X3	S3	0.0888(15)	0.08674(11)	0.45222(21)	1	0.0608(42)	0.0634(29)	0.0721(33)	−0.0039(24)	−0.0011(52)	−0.0076(47)	0.0666(16)
X4	S4	0.5907(14)	0.08786(11)	0.4529(2)	1	0.0612(40)	0.0582(27)	0.0672(31)	−0.0035(23)	0.0025(51)	−0.0098(47)	0.0630(15)
X5	S5	0.0972(14)	0.1612(1)	0.4522(2)	1	0.0577(38)	0.0595(29)	0.0753(33)	0.0029(24)	0.0096(67)	0.0086(55)	0.0642(14)
X6	S6	0.5963(14)	0.16110(11)	0.45543(21)	1	0.0569(39)	0.0632(30)	0.0775(34)	0.0041(24)	0.0082(67)	0.0056(56)	0.0661(14)
X7	S7	0.4607(13)	0.2919(1)	0.67188(18)	1	0.0480(31)	0.0508(25)	0.0577(27)	0.0004(20)	−0.0040(55)	−0.0092(51)	0.0534(12)
X8	S8	0.5405(12)	0.2078(1)	0.32414(17)	1	0.0461(30)	0.0514(25)	0.0574(28)	−0.0018(19)	−0.0018(53)	−0.0088(51)	0.0527(12)
X9	S9	0.0355(13)	0.12354(9)	0.34308(19)	0.4	0.0481(38)	0.0454(22)	0.0563(28)	0.0000(18)	0.0164(47)	−0.0023(28)	0.0490(13)
	Cl9	0.0355(13)	0.12354(9)	0.34308(19)	0.6	0.0481(38)	0.0454(22)	0.0563(28)	0.0000(18)	0.0164(47)	−0.0023(28)	0.0490(13)
X10	S10	0.5304(11)	0.12330(8)	0.34359(17)	0.4	0.0406(39)	0.0354(19)	0.0469(25)	−0.0025(16)	0.0125(39)	−0.0017(24)	0.0404(13)
	Cl10	0.5304(11)	0.12330(8)	0.34359(17)	0.6	0.0406(39)	0.0354(19)	0.0469(25)	−0.0025(16)	0.0125(39)	−0.0017(24)	0.0404(13)
X11	S11	0.0391(12)	0.03780(9)	0.32592(17)	1	0.0442(29)	0.0459(22)	0.0594(28)	−0.0018(19)	−0.0109(52)	0.0037(48)	0.0518(12)
X12	S12	0.4645(12)	0.9617(1)	0.67697(18)	1	0.0474(31)	0.0520(24)	0.0655(31)	0.0003(20)	−0.0129(55)	0.0063(51)	0.0572(13)
X13	S13	0.75859(63)	0.08595(9)	0.24962(23)	0.4	0.0635(35)	0.0512(22)	0.0691(31)	0.0003(21)	−0.0031(81)	0.0010(22)	0.0627(13)
	Cl13	0.75859(63)	0.08595(9)	0.24962(23)	0.6	0.0635(35)	0.0512(22)	0.0691(31)	0.0003(21)	−0.0031(81)	0.0010(22)	0.0627(13)
X14	S14	0.75627(62)	0.16051(9)	0.25043(21)	0.4	0.0625(36)	0.0526(23)	0.0726(32)	−0.0018(23)	−0.0030(87)	0.0030(23)	0.0640(13)
	Cl14	0.75627(62)	0.16051(9)	0.25043(21)	0.6	0.0625(36)	0.0526(23)	0.0726(32)	−0.0018(23)	−0.0030(87)	0.0030(23)	0.0640(13)
X15	S15	0.3891(14)	0.0611(1)	0.55286(19)	1	0.0533(40)	0.0561(26)	0.0612(28)	0.0041(21)	0.0080(48)	0.0012(38)	0.0570(14)
X16	S16	0.92039	0.0622(1)	0.5552(2)	1	0.0578(49)	0.0547(27)	0.0641(30)	0.0031(21)	0.0097(48)	0.0020(37)	0.0588(17)
X17	S17	0.62375(75)	0.9795(1)	0.56392(19)	1	0.0455(42)	0.0516(24)	0.0541(28)	−0.0003(20)	0.0156(30)	0.0026(24)	0.0496(15)
X18	S18	0.8454(12)	0.02004(10)	0.43555(19)	1	0.0654(39)	0.0611(27)	0.0711(33)	−0.0015(23)	0.0260(51)	−0.0007(41)	0.0642(14)
X19	S19	0.7202(10)	0.03151(9)	0.66812(17)	0.7	0.0594(33)	0.0506(24)	0.0565(26)	0.0034(19)	0.0118(39)	0.0001(35)	0.0552(12)
	Cl19	0.7202(10)	0.03151(9)	0.66812(17)	0.3	0.0594(33)	0.0506(24)	0.0565(26)	0.0034(19)	0.0118(39)	0.0001(35)	0.0552(12)
X20	S20	0.16455(61)	0.0322(1)	0.6688(2)	1	0.0484(39)	0.0473(24)	0.0574(28)	0.0001(20)	0.0109(27)	0.0038(22)	0.0507(15)
X21	S21	0.24528(83)	0.22647(11)	0.6700(2)	1	0.0613(55)	0.0590(26)	0.0654(32)	0.0028(23)	0.0116(33)	0.0002(28)	0.0617(19)
X22	S22	0.67252(8)	0.22546(11)	0.6697(2)	1	0.0611(54)	0.0561(27)	0.0667(33)	0.0028(23)	0.0104(33)	−0.0031(27)	0.0613(19)
X23	S23	0.383058(73)	0.22729(12)	0.4391(2)	1	0.0510(45)	0.0578(27)	0.0580(30)	−0.0030(21)	0.0159(31)	0.0019(26)	0.0548(17)
X24	S24	0.8333(12)	0.22672(11)	0.4404(2)	1	0.0633(40)	0.0667(30)	0.0732(35)	−0.0020(24)	0.0034(46)	−0.0009(43)	0.0685(16)
X25	S25	0.37343(83)	0.184088(9)	0.56052(18)	1	0.0488(49)	0.0484(25)	0.0560(27)	−0.0043(19)	0.0133(30)	−0.0057(23)	0.0505(17)
X26	S26	0.93754(2)	0.1855(1)	0.56139(19)	1	0.0586(56)	0.0561(27)	0.0579(29)	−0.0050(22)	0.0080(33)	−0.0007(27)	0.0576(19)
X27	S27	0.93119(78)	0.15955(12)	0.69259(24)	1	0.0683(53)	0.0659(32)	0.0773(35)	0.0030(25)	0.0258(34)	0.0018(27)	0.0690(19)
X28	S28	0.49753(81)	0.1543(1)	0.69639(19)	1	0.0422(37)	0.0502(23)	0.0667(29)	0.008(2)	0.0097(31)	−0.0001(25)	0.0529(14)
X29	Cl29	0.5	0.03412(14)	0.75	1	0.0589(44)	0.0600(36)	0.0594(39)	0.00000	0.0106(54)	0.00000	0.0593(17)
X30	Cl30	0	0.22146(15)	0.75	1	0.0625(45)	0.0619(39)	0.0770(47)	0.00000	0.0102(59)	0.00000	0.0672(18)
X31	S31	0.24678	0.10002(9)	0.74732(19)	0.7	0.0536(35)	0.0567(23)	0.0681(28)	0.0004(23)	0.0097(78)	−0.0008(22)	0.0594(11)
	Cl31	0.24678	0.10002(9)	0.74732(19)	0.3	0.0536(35)	0.0567(23)	0.0681(28)	0.0004(23)	0.0097(78)	−0.0008(22)	0.0594(11)

Note: s.o.f. indicates the site occupancy factor.

TABLE 7. Selected interatomic distances (Å) for tazieffite

Pb1-	S2	2.874(10)	Pb2-	S1	2.913(10)
	S4	2.954(9)		S16	2.941(5)
	S15	2.974(5)		S3	2.981(9)
	S6	3.089(9)		S2	3.037(11)
	S25	3.147(5)		S4	3.140(9)
	S1	3.147(11)		S5	3.153(9)
	S3	3.184(9)		S26	3.214(5)
	S5	3.250(9)		S6	3.225(9)
Pb3-	S11	2.895(8)	Pb4-	S11	2.910(8)
	S12	2.918(8)		S12	2.924(8)
	S17	2.945(5)		S18	2.929(5)
	S4	3.033(9)		S3	3.001(9)
	S10	3.123(7)		S4	3.153(9)
	S3	3.142(10)		X9	3.173(8)
	X9	3.282(8)		X10	3.306(7)
	X13	3.337(5)		X13	3.366(5)
Pb5-	S7	2.892(8)	Pb6-	S8	2.906(8)
	S8	2.970(8)		S7	2.920(9)
	S5	3.033(9)		S5	2.999(9)
	S23	3.043(5)		S24	3.004(5)
	S6	3.046(9)		S6	3.089(9)
	X10	3.114(7)		X9	3.160(8)
	X9	3.246(8)		X10	3.283(7)
	X14	3.404(5)		X14	3.397(5)
Pb7-	S29	2.947(5)	Pb8-	S21	2.917(5)
	X19	2.967(5)		S22	2.955(5)
	S20	3.014(5)		Cl30	2.975(5)
	S12	3.074(7)		S8	3.027(8)
	S12	3.101(8)		S8	3.063(7)
	S11	3.155(8)		S7	3.174(8)
	S11	3.180(7)		S7	3.178(8)
	X13	3.366(4)		X14	3.219(4)
(Pb,NH₄)9-	S1	2.981(10)	(Pb,NH₄)10-	S2	3.072(10)
	S20	3.083(5)		S28	3.092(5)
	S16	3.113(5)		X31	3.127(6)
	S31	3.121(5)		S1	3.195(10)
	S2	3.171(10)		X31	3.213(5)
	X31	3.272(6)		S15	3.259(5)
	X19	3.310(6)		X19	3.418(6)
	S27	3.355(6)		Cl29	3.427(5)
				S20	3.598(5)
Bi11-	S27	2.501(7)	As11-	S27	2.302(7)
	S28	2.692(6)		S28	2.391(7)
	S27	2.876(6)		X31	2.416(5)
	Cl30	2.878(5)		S28	2.765(7)
	S28	2.887(7)		S27	2.871(7)
	S21	3.069(6)		Cl30	3.731(6)
	S22	3.197(6)		S22	3.945(6)
	X31	3.500(5)		S21	4.016(6)
Cd1a/Pb1b/ Sn1c-	X9	2.508(5) x2	Cd2a/Pb2b/ Sn2c-	X10	2.524(5) x2
	X13	2.632(5) x2		X14	2.731(5) x2
	X14	2.655(5) x2		X13	2.749(5) x2
Bi1a/As1b-	S8	2.539(5)	As1-	S21	2.307(8)
	S23	2.799(6)		S22	2.354(8)
	S22	2.807(7)		S7	2.397(6)
	S21	2.812(7)		S24	3.108(10)
	S24	2.947(8)		S23	3.194(8)
	S26	3.231(5)		S25	3.372(6)
As2a-	S6	2.436(7)	Bi2b-	S5	2.531(5)
	S23	2.480(9)		S26	2.700(7)
	S24	2.696(12)		S25	2.728(6)
	S25	3.060(10)		S24	2.805(8)
	S26	3.137(10)		S23	3.022(6)
	S24	3.403(7)		S23	3.349(6)
Bi2a/As2b-	S6	2.349(10)	As3a-	S1	2.308(7)
	S23	2.422(13)		S25	2.519(10)
	S24	2.514(16)		S26	2.595(9)
	S26	3.187(13)		S21	3.087(7)
	S25	3.243(14)		S28	3.099(7)
	S24	3.506(10)		S27	3.176(10)
Bi3b-	S25	2.584(11)	Bi4a/As4b-	S2	2.529(6)
	S26	2.612(11)		S27	2.679(6)
	S1	2.673(8)		S28	2.823(6)
	S21	2.716(7)		S25	2.913(6)
	S28	3.063(11)		S26	2.992(7)
	S27	3.084(12)		S22	2.995(5)

TABLE 7.—CONTINUED

As5a-	S3	2.359(8)	Bi5b-	S3	2.485(7)
	S16	2.489(16)		S16	2.647(13)
	S15	2.514(16)		S15	2.665(13)
	S18	2.972(13)		S18	2.805(12)
	S17	3.213(13)		S17	3.064(11)
	S18	3.385(7)		S18	3.249(7)
Bi6a/As6b-	S4	2.483(5)	As7a-	S20	2.309(9)
	S17	2.637(5)		X19	2.439(11)
	S15	2.772(10)		S11	2.444(6)
	S16	2.883(10)		S18	3.045(11)
	S18	2.893(9)		S16	3.153(6)
	S17	3.305(5)		S17	3.212(9)
Bi7b-	S11	2.481(8)	Bi8a/As8b-	S12	2.508(5)
	S20	2.543(13)		S17	2.731(6)
	S18	2.708(16)		X19	2.767(7)
	X19	2.753(15)		S18	2.878(8)
	S17	2.997(15)		S20	2.965(6)
	S16	3.103(8)		S15	3.124(5)

NH_4Cl, and lafossaite, TlCl, which show almost the same unit-cell parameters (Roberts et al. 2006).

In the structure of tazieffite, Cd atoms, mixed with Pb and Sn atoms, were assigned to M12 and M13, which form [100] single columns of edge-sharing octahedra along the axis of the lozenge-shaped rods. According to bond valences, the two pairs of anion positions in the (001) octahedral plane, i.e., X13 and X14, as well as the two atom positions at the octahedral vertex along [001], i.e., X9 and X10, show a mixed (S,Cl) occupancy with Cl dominating over S. The octahedral environments of M12 and M13 are almost regular with a pair of cation-anion distances along [001] equal to 2.508(5) and 2.524(5) Å for M12 and M13, respectively; the pairs of opposing bonds in the $M(Cl,S)_4$ plane (001) are equal to 2.632(5)–2.655(5) Å for M12 and to 2.731(5)–2.749(5) Å for M13. The calculated ECCv is 0.02 and 0.016 for M12 and M13, respectively (Table 8). These values are considerably lower than those calculated for the corresponding positions in the structure of vurroite (0.2589 and 0.3332, respectively), thus indicating that the position of the central cation in the coordination polyhedra M12 and M13 of tazieffite is more symmetric than in the corresponding octahedra of vurroite. This feature is related to the absence of the element with more a pronounced stereoactive-lone-pair effect (Bi) in the octahedrally coordinated sites of tazieffite. The presence of Pb instead of Bi in these cation positions is strongly suggested by the regularity of the resulting octahedra. As suggested by Doussier et al. (2008), in a chemically complex structure, the less electro-negative cation has the highest affinity for the most electro-negative anion (here, Cl with respect to S). Thus, in a complex compound, besides geometric (steric) aspects and a local charge balance, one has to consider also chemical affinities. In the case of tazieffite, Cd is the less electro-negative cation (Pauling electronegativity equal to 1.7), followed by Pb and Sn (1.8), Bi (1.9), and finally As (2.0). As a consequence, Cd, together with Pb and Sn, has a stronger affinity for Cl (Pauling electro-negativity equal to 3.0, whereas S has 2.5) than does As (or Bi). The resulting difference in bond character is barely 10% on the ionicity scale of Pauling (1960), so that this influence will be limited. Especially in the case of Sn^{4+}, it is the local charge balance that will dictate the resulting coordination. Still, in the compound $Sn_2S_3Cl_2$ (Batsanov et al. 1966), tetravalent Sn is expected to form bonds with both Cl and S.

**TABLE 8.** Coordination parameters for cation sites of tazieffite

Atom/site	C.N.	<d>	dmin	dmax	Vs	ECC$_v$	SPH$_v$	Vp	υ	Valence†
Pb1	8	3.08(13)	2.874(10)	3.250(9)	122.248	0.1845	0.9811	51.20(33)	0.0339	2.03
Pb2	8	3.08(12)	2.913(10)	3.225(9)	122.573	0.1726	0.9684	51.01(33)	0.0400	2.03
Pb3	8	3.08(17)	2.895(8)	3.337(5)	122.623	0.2057	0.9111	51.13(30)	0.0381	2.03
Pb4	8	3.10(18)	2.910(8)	3.366(5)	123.904	0.2307	0.9165	51.69(29)	0.0376	2.00
Pb5	8	3.09(16)	2.892(8)	3.404(5)	123.633	0.1646	0.8853	51.29(29)	0.0430	1.96
Pb6	8	3.10(18)	2.906(8)	3.397(5)	123.925	0.2028	0.8959	51.30(29)	0.0450	1.98
Pb7	8	3.10(14)	2.947(5)	3.366(4)	124.476	0.1736	0.9585	50.70(27)	0.0604	1.88
Pb8	8	3.06(11)	2.917(5)	3.219(4)	120.546	0.1518	0.9633	49.32(27)	0.0561	2.06
Pb9/(NH$_4$)9	8	3.18(13)	2.981(10	3.355(6)	134.556	0.1588	0.9370	55.98(32)	0.0402	1.55
Pb10/(NH$_4$)10	9	3.27(18)	3.072(10)	3.598(5)	144.561	0.2229	0.9299	69.30(35)	0.0174	1.41
Bi11	8	2.95(31)	2.501(5)	3.500(5)	108.456	0.1228	0.6994	42.29(24)	0.1004	2.98
As11	8	3.06(73)	2.302(7)	4.016(6)	108.456	0.7337	0.6994	42.29(24)	0.1004	2.98
Cd1a/Pb1b/Sn1c	6	2.60(07	2.508(5)	2.655(5)	73.510	0.0200	0.9192	23.00(13)	0.0170	3.21
Cd2a/Pb2b/Sn2c	6	2.67(11)	2.524(5)	2.749(5)	79.559	0.0162	0.8746	24.54(14)	0.0308	2.89
Bi1a/As1b	6	2.86(23)	2.539(5)	3.231(5)	98.812	0.3311	0.9564	29.83(18)	0.0515	2.55
As1	6	2.79(49)	2.307(8)	3.372(6)	97.203	0.6366	0.9154	28.53(17)	0.0781	2.58
Bi2a/ As2b	6	2.86(29)	2.531(5)	3.349(6)	102.173	0.4024	0.9457	30.54(18)	0.0610	2.69
As2a	6	2.87(50)	2.349(10)	3.506(10)	104.775	0.6276	0.9646	31.17(18)	0.0654	2.75
Bi2b	6	2.87(39)	2.436(7)	3.403(7)	104.776	0.5187	0.9646	31.17(18)	0.0654	2.75
As3a	6	2.80(37)	2.308(7)	3.176(10)	92.592	0.4928	0.9117	28.54(17)	0.0317	2.40
Bi3b	6	2.79(23)	2.584(11)	3.084(12)	92.592	0.3302	0.9117	28.54(17)	0.0317	2.40
Bi4a/As4b	6	2.82(19)	2.529(6)	2.995(5)	94.852	0.2726	0.9271	29.14(17)	0.0349	2.56
As5a	6	2.82(43)	2.359(8)	3.385(7)	97.430	0.5668	0.9383	29.54(19)	0.0476	2.55
Bi5b	6	2.82(29)	2.485(7)	3.249(7)	97.430	0.4035	0.9383	29.54(19)	0.0476	2.55
Bi6a/As6b	6	2.83(28)	2.483(5)	3.305(5)	98.073	0.3945	0.9489	29.77(19)	0.0465	2.66
As7a	6	2.77(41)	2.309(9)	3.212(9)	90.644	0.5836	0.9720	27.68(17)	0.0406	2.66
Bi7b	6	2.76(25)	2.481(8)	3.103(8)	90.647	0.3750	0.9720	27.68(17)	0.0407	2.66
Bi8a/As8b	6	2.83(21)	2.508(5)	3.124(5)	95.497	0.3070	0.9846	29.50(19)	0.0296	2.56

Notes: <d> = average bond distance, Vs = volume of the circumscribed sphere, ECC$_v$ = volume eccentricity of the coordination, SPH$_v$ = volume sphericity of the coordination, Vp = volume of the coordination polyhedron, υ = volume distortion.
* The polyhedron parameters for atomic coordinations are defined in Balić-Žunić and Makovicky (1996) and in Makovicky and Balić-Žunić (1998). All calculations were done with the program IVTON (Balić-Žunić and Vicković 1996).
† Bond valence parameters of Brese and O'Keeffe (1991) were used. For the mixed sites, the calculated valences of individual species are multiplied by the fractional occupancies and summed.

Taking into account the above remarks, it is possible to assume that in the mixed (Cl,S) sites forming the (Cd,Pb,Sn)-centered polyhedra of the tazieffite structure, S is favored when Sn^{4+} is bound with these anion positions, whereas Cl is favored when bound to Cd and Pb. In accordance with overall charge balance, these ligands are primarily Cl. This situation is different from that in vurroite, in which the cation sites M12 and M13 are occupied by Sn^{4+} and Bi^{3+}, and no significant Cl is present in their
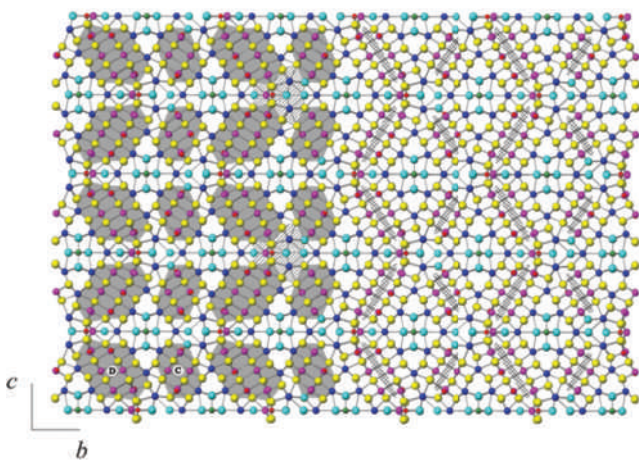
octahedral environment. According to Pinto et al. (2008), only 0.03 atom of Cl substitutes for S in the same anion sites. Bond valence calculations permit the assumption that in the structure of vurroite minor Cl may substitute for S only into the two sites S13 and S14 of the octahedral environment of M12 and M13. As a matter of fact, the bond valences calculated for S13 and S14 in vurroite correspond to 1.60 and 1.67, respectively, which are values lower than those expected for a pure S site, but significantly higher than those calculated for the corresponding positions in the structure of tazieffite (i.e., 1.20 and 1.22, respectively).

On the two opposite sides of the lozenge-shaped rods, the repetition along [100] of the As and Bi pyramids forms trapezoidal ribbons with thicknesses of two (ribbon 2R) and three (ribbon 3R) trapezoids, respectively (Fig. 5). All but As1 site show a mixed (Bi,As) occupancy with different preferences for As or Bi in each site (Fig. 5), but with a total As occupancy exceeding that of Bi. Among these mixed positions, a very strong preference for As is observed in the positions M22 and M18, followed by M20 and M17. In M14, M16, M19, M23, and M21, Bi dominates. As1 shows an As-S distance to the apex of the pyramid equal to 2.397(6) Å, whereas the two pairs of opposing bonds at the base of the pyramid are 2.307(8)–3.108(10) and 2.354(8)–3.194(8) Å, respectively. Cation-to-ligand distances in the mixed (Bi,As) positions are intermediate between those expected for full As and Bi polyhedra, being closer to typical As-S or Bi-S distances (see vurroite; Pinto et al. 2008), in agreement with refined site occupancy factors.

Bond-valence calculations on anions showed that Cl atoms appear to concentrate among some anion positions having z
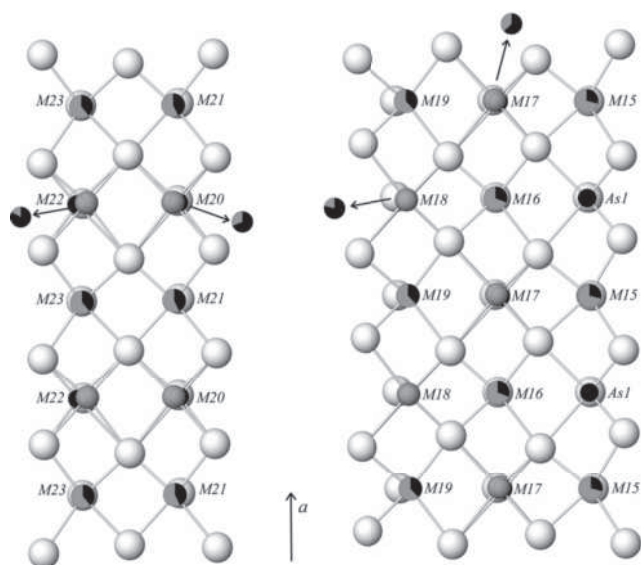

FIGURE 4. A global view of the structure of tazieffite down [100], with PbS-like rods (shaded gray) and lone-electron pair micelles (cross-hatched) outlined. Two of the groups of trigonal prisms in the so-called "constricted portion" of the structure are also indicated (hatched).

FIGURE 5. Trapezoidal ribbons of As and Bi atoms projected perpendicular to [100] and the planes of ribbons. Black and dark gray indicate respectively the percentage of As and Bi occupancies of the site.

equal or close to ¼ and ¾ (see the refinement paragraph), without Cl on other positions (Table 5). This suggests that the total Cl content (together with minor Br and I) given by microprobe analysis (about 8 for a total of 60 anions) is distributed exclusively among these anion positions. Thus, the thin "chlorinated" layer at $z \sim$ ¼ and ¾ acts like a twin plane connecting the two types of sulfide rods (rods C and D in Fig. 4) along the **c** direction. The structure is chemically similar to a composite layered structure where a thick sulfide slab (with minor Cl) alternates with a thinner, Cl-rich layer.

A survey of halogen-sulfide structures reveals several types of role for halogens in simple or complex compounds containing lone-electron-pair elements such as Sn, Sb, and Bi: (1) they may be present as anion columns in 1D channels [e.g., synthetic $Bi(Bi_2S_3)_9I_3$ (Miehe and Kupčík 1971) and pillaite, $Pb_9Sb_{10}S_{23}ClO_{0.5}$ (Orlandi et al. 2001; Meerschaut et al. 2001)]; (2) they may form parts of coordination polyhedra of large (Pb) cations [e.g., dadsonite, $Pb_{23}Sb_{25}S_{60}Cl$ (Moëlo 1979; Makovicky et al. 2006), synthetic $Pb_{3+x}Sb_{3-x}S_{7+x}Cl_{1+x}$ (Doussier et al. 2008), and mutnovskite, $Pb_2AsS_3(I,Cl,Br)$ (Zelenski et al. 2006)]; (3) they may form complete coordination polyhedra of Sn^{2+} or Bi^{3+} (e.g., synthetic Sn_4SI_6, Fenner 1978); and finally, (4) they may partake in the coordination polyhedra of metalloids as ligands forming longer and weaker M-(Cl,Br,I) bonds with respect to the three shorter and stronger M-S bonds [e.g., synthetic BiSCl (Voutsas and Rentzeperis 1980), synthetic Sn_2SI_2 (Thévet et al. 1976), and synthetic $Cu_3Bi_2S_3I_3$ (Balić-Žunić et al. 2005)]. Recently, two natural analogues of the Bi-halogeno-sulfides BiSCl (IMA no. 2008-020) and BiSBr (Demartin et al. 2008) belonging to the last category have been discovered at Vulcano, but no As halogeno-sulfide (natural or synthetic) is known to date.

If we disregard the questionable minor content of Cl in the S19 site, tazieffite belongs to the second group although the Cl-

rich columns of (Cd, Sn, Pb) octahedra may also be interpreted as an augmented version of anion columns from the first category, analogous to that in the synthetic Mn-Pb-Sb oxy-chloro-sulfide $(Mn_{1-x}Pb_x)Pb_{10+y}Sb_{12-y}S_{26-y}Cl_{4+y}O$ (Doussier et al. 2007). The S content of the S31 site matches the As content of the mixed As11-Bi11 polyhedron; its Cl content is correlated with the presence of a long, non-bonded Bi-X distance that cannot be counted as a Bi-X bond.

Similar to tazieffite, in many of these structures modular analysis shows a spatial segregation of cations and anions into linear or planar sub-domains.

Relation to vurroite

Tazieffite is closely related to the halogen-sulfosalt vurroite $Pn_{20}Sn_2Bi_{22}S_{54}Cl_6$ (Garavelli et al. 2005; Pinto et al. 2008) both from a chemical and structural point of view. The most significant chemical differences observed in tazieffite are: (1) the presence of Cd substituting for Sn; (2) As content exceeding Bi; (3) higher Cl and Se content; and (4) the consistent presence of minor I. Thus, tazieffite can be considered as the (Cd,As)-dominant isotype of vurroite.

The presence of Cd in this mineral is of particular interest. Due to the difference in the valence state of Cd(2+) and Sn(4+), a coupled heterovalent substitution $Sn^{4+} + 2S^{2-} \rightarrow Cd^{2+} + 2Cl^-$ occurs in tazieffite. This constitutes the main contribution to the observed higher Cl content of this mineral with respect to vurroite.

In the structure of tazieffite, Cd represents the dominant cation (over Sn and Pb) in the octahedral sites M12 and M13, whereas Sn dominates over Bi in the corresponding positions of vurroite. Nevertheless, microprobe data (Table 2) show that, in the analyzed samples from Kamchatcha, the content of Cd does not exceed 1 apfu. As a consequence, the simplified formula for the investigated samples of tazieffite can be written as $Pb_{20}(Cd,Sn,Pb)_2(As,Bi)_{22}S_{52}Cl_8$. However, one cannot exclude the existence in natural material of tazieffite samples with Cd-richer compositions, which may extend up to complete substitution of Sn and Pb by Cd. Thus, the simplified putative end-member formula of tazieffite can be written as $Pb_{20}Cd_2(As,Bi)_{22}S_{50}Cl_{10}$.

The structure refinement showed that the so-called ribbons 2R and 3R of the structure of tazieffite do not show an ordering of Bi and As atoms, either along the ribbon axis ([100]) or in the direction perpendicular to it. This is in contrast with the situation observed in the structure of vurroite, in which an almost complete alternation between Bi and As in every second coordination polyhedron was observed. According to Pinto et al. (2008), this alternation facilitates stability in the structure that should contain both As and Bi in comparable amounts. However, in the case of vurroite a surplus of Bi was observed, which suggested a limited Bi/As solid-solution behavior in the ribbons. In the structure of tazieffite, the mixed (Bi,As) occupancy observed in most of cation sites of the ribbons indicates a high degree of As/Bi solid solution among these sites, which can be ascribed to the As-richer composition of this mineral relative to vurroite, and may be connected with the higher degree of structural disorder observed. The extension of the solid solution also into the As-dominated compositions has been already predicted by Pinto et al. (2008).

DISCUSSION

Tazieffite is a new example of a multicomponent complex sulfosalt in which Cl (partly replaced by I and Br) and Cd (partly replaced by Sn) act as essential constituents, together with Pb, Bi, As, and S. In spite of the relative abundance of sulfosalt species containing halogens (Moëlo 1979; Breskovska et al. 1982; Orlandi et al. 2001, 2004; Garavelli et al. 2005; Zelenski et al. 2006), tazieffite is just the second sulfosalt, together with kudriavite, containing Pb, Cd, and Bi to be found in nature and the first one having also As as essential constituent. According to both chemical and structural data, tazieffite has no analogues among synthetic compounds. Nonetheless, it can be considered the Cd-rich isotypic derivative of the mineral vurroite, $Pb_{20}Sn_2(Bi,As)_{22}S_{54}Cl_6$ (Garavelli et al. 2005; Pinto et al. 2008), according to the heterovalent substitution $Sn^{4+} + 2S^{2-} \rightarrow Cd^{2+} + 2Cl^-$.

Recent studies have shown that the presence of Cd as minor component in sulfosalts is more common than previously believed. For instance, Pattrick (1978) reported Cd-rich varieties of tetrahedrite, $\sim Cu_{10}Cd_2Sb_4S_{13}$ and, according to Moëlo et al. (1984, 1989), Cd would be an essential component of ramdohrite, ideally $CdPb_{12}Ag_{5.5}Sb_{21.5}S_{48}$. Up to now, the sole natural representative of Cd-Pb-Bi sulfosalts was the mineral kudriavite $(Cd,Pb)Bi_2S_4$ (Chaplygin et al. 2005), discovered in sublimates from high-temperature fumaroles of Kudriavy volcano (Iturup Island, Kurile Arc, Russia) and found also at Mutnovsky in association with Cd-rich cannizzarite and tazieffite. The presence of Cd in sublimates from Mutnovsky is connected with its abundance in the volcanic gas phase (Zelenski and Bortnikova 2005). Moreover, small amounts of Cd were also reported in sulfosalts from "La Fossa" crater (Vulcano Island, Italy), where this element substitutes for Pb in lillianite (up to 0.28 wt%), in mozgovaite (up to 0.26 wt%), and in heyrovskýite (up to 0.4 wt%) (Borodaev et al. 2001, 2003; Vurro et al. 1999).

The presence of Cl in tazieffite as the predominant halogen allows us to consider this mineral as a new chloro-sulfosalt, in addition to ardaite ($Pb_{10}Sb_6S_{17}Cl_4$; Breskovska et al. 1982), dadsonite ($Pb_{23}Sb_{25}S_{60}Cl$; Moëlo 1979), pillaite ($Pb_9Sb_{10}S_{23}ClO_{0.5}$; Orlandi et al. 2001) and pellouxite [$(Cu,Ag)_2Pb_{21}Sb_{23}S_{55}ClO$; Orlandi et al. 2004].

The presence of minor I substituting for Cl is particularly interesting and makes tazieffite the second example, after mutnovskite (Zelenski et al. 2006), of natural I-bearing sulfosalt. It is noteworthy that both mutnovskite and tazieffite come from the same fumarole deposit and formed under very similar conditions. In the environment of formation, tazieffite forms after greenockite, kudriavite, and Cd-rich cannizzarite but before mutnovskite, as is testified by the paragenetic sequence of deposition observed in hand specimens from which the phases were collected. As in other epithermal deposits, the key factors governing the deposition of these phases are the abundance of the metal elements in the fumarole steam and the combination of appropriate temperatures and partial-pressures of S, O, and halogens. The importance of the halogens is mainly due to their role as carriers for the metals but also as catalyst for the reactions of deposition of sulfosalts (Quisefit et al. 1989; Symonds et al. 1987, 1992; Symonds and Reed 1993; Garavelli et al. 1997; Cheynet et al. 2000). With the exception of mutnovskite, which has never been found inside the sampling tubes, the observed sequence of deposition of minerals on the ground is the same as observed for sublimates in silica tubes inserted in the same fumaroles from which tazieffite formed (Zelenski and Bortnikova 2005). Taking into account what was previously observed for mutnovskite (Zelenski et al. 2006), the similarity of the deposition sequence could be explained with a quite stable chemical composition, temperature and flux rate of fumarole fluids discharging from Mutnovsky volcano for the duration of deposition. This contrasts with what happens in other epithermal deposits where the composition of fluids has been found to change instantaneously (Borodaev et al. 2003).

Chlorine and, very subordinately, Br are common halogen elements in volcanic fluids discharging from fumaroles. In contrast, I concentrations, which are even lower than those of Br, are almost completely exclusive to arc volcanoes and they vary widely through time for individual volcanoes and from volcano to volcano (Aiuppa et al. 2005 and references therein). If, on the one hand, this behavior justifies the overall global scarcity of I-bearing sublimates, on the other hand it explains the particular concentration of I-rich phases at Mutnovsky volcano. This is in fact one of the most active volcanoes of the Kuril-Kamchatka arc, whose geological context corresponds to volcanic arc tectonic settings, where volcanic fluids are expected to be enriched in I, due to the recycling of marine sedimentary components (Muranatsu and Wedepohl 1998).

According to Zelenski and Bortnikova (2005), a large variety of I-bearing phases was deposited in silica sampling tubes deeply inserted in fumarole vents around which tazieffite formed in fissures and cavities on the ground. Thallium iodide or complex halides are reported as the most abundant I-rich phases collected in the tubes, but I content was found to be important also for some sulfo-halide compounds like BiS(Cl,I,Br) or AsS(Cl,I,Br). This evidence is important in discussing the problem of the formation of tazieffite. Zelenski and Bortnikova (2005) reported the occurrence in silica tubes of a halogen-bearing sulfosalt very similar to tazieffite, both from a chemical and morphological point of view. The authors described this phase with the formula $Pb_3(As,Bi)_3S_7Cl$, which shows atomic ratios very similar to those of tazieffite although no Cd was reported for the former. Actually, up to 2.0 at% Cd was found in $Pb_3(As,Bi)_3S_7Cl$. The close chemical and morphological similarity between the Pb-Bi-As chloro-sulfosalt found in the silica tubes and the samples of tazieffite from the ground, as well as the analogy of the X-ray powder pattern, indicate that they correspond to the same mineral phase. In the silica sampling tubes, the majority of tazieffite forms approximately from 380 °C down to about 250 °C, which is quite the same range of temperature measured in fumaroles around which tazieffite crystallized on the ground; it occurs in radiating acicular aggregates associated with small amounts of PbS, small kirkiite crystals, and various complex halides and sulfo-halides of Cd, NH_4, Pb, and Bi. These phases sometimes contain noticeable As and I (e.g., up to 24 wt% of I in the $Bi_3S_3ClI_2$ phase). Thermo-chemical calculations have shown that high-temperature transport of metals at Mutnovsky volcano occurs as halides or sulfides (Zelenski 2003; Zelenski and Bortnikova 2005). The same process was also observed in other active volcanoes (Bernard and Le Guern 1986; Symonds et

al. 1987; Quisefit et al. 1989; Symonds 1993), but especially in the volcanic apparatus of La Fossa crater at Vulcano (Garavelli 1994; Cheynet et al. 2000). The latter volcano produced, in the years 1991–1998, a high-temperature sublimate deposition very close to that of Mutnovsky volcano, characterized by complex Pb-Bi-As sulfosalts and halogen sulfosalts (Garavelli et al. 2005; Pinto et al. 2006). Notwithstanding the limitations imposed by thermodynamic simulators, which operate only with very simple species, thermo-chemical calculations (Cheynet et al. 2000; Zelenski and Bortnikova 2005) suggest that complex Pb-Bi-As sulfosalts were deposited by gas-solid reaction of simple binary MeS or MeX (Me = metal, X = halogen) compounds or complex MeSX species, which condensed forming simple or complex solids depending on the conditions of the system (i.e., temperature, partial-pressure of S, O, and halogens, presence of trace elements, and so on). In the fumarolic depositional environment of Mutnovsky, tazieffite could be formed from simple metal sulfides (PbS, CdS) as well as from complex sulfohalides of Bi and As, which change into sulfosalts under the action of gaseous HCl and H_2S. It is noteworthy that solid CdS, PbS, and Bi-As-S-Cl-I-Br compounds have been identified among sublimates deposited on the inner walls of silica tubes (Zelenski and Bortnikova 2005), and greenockite and galena have been also identified among sublimates from the ground. In addition, another chloride, NH_4CdCl_3, was described from the tubes. This is important because it indicates a relatively high ammoniac fugacity in the fumarole gases at Mutnovsky. Thus one can hypothesize that at high temperature, gaseous NH_3 and gaseous HCl combine with solid CdS or gaseous $CdCl_2$ to form NH_4CdCl_3; at lower temperature, gaseous NH_3 contributes to the formation of NH_4BF_4, whose occurrence is also reported in the coldest portions of the silica tubes (Zelenski and Bortnikova 2005). The above evidence suggests the possible presence of NH_4^+ in other compounds formed at intermediate temperatures, thus supporting our conclusion that small amounts of NH_4^+ are effectively incorporated in the crystal structure of tazieffite.

Finally, the possibility that solid NH_4CdCl_3 previously formed could be directly involved in the formation of tazieffite also cannot be excluded. A possible reaction could be the following: $20PbS(s) + 2NH_4CdCl_3 + 11(Bi,As)_2S_3 + 6HCl \rightarrow Pb_{20}Cd_2(As,Bi)_{22}S_{50}Cl_{10} + 2NH_4Cl + 3H_2S$. Solid NH_4CdCl_3 was observed in the tubes among sublimates deposited at temperature of about 460–440 °C and from 300 to 200 °C. Solid NH_4CdCl_3 was not spatially associated with sulfosalts, and it is present only where sulfosalts are absent. This indirectly confirms the hypothesis of tazieffite formation through an intermediate product like NH_4CdCl_3.

REFERENCES CITED

Aiuppa, A., Federico, C., Franco, A., Giudice, G., Guerrieri, S., Inguaggiato, S., Liuzzo, M., McGonigle, A.J.S., and Valenza, M. (2005) Emission of bromine and iodine from Mount Etna volcano. Geochemistry Geophysics Geosystems, 6, 1–8.

Balić-Žunić, T. and Makovicky, E. (1996) Determination of the centroid or "the best centre" of a coordination polyhedron. Acta Crystallographica, B52, 78–81.

Balić-Žunić, T. and Vicković, I. (1996) IVTON—a program for the calculation of geometrical aspects of crystal structures and some crystal chemical applications. Journal of Applied Crystallography, 29, 305–306.

Balić-Žunić, T., Mariolacos, K., Friese, K., and Makovicky, E. (2005) Structure of a synthetic halogen sulfosalt, $Cu_3Bi_2S_3I_3$. Acta Crystallographica, B61, 239–245.

Batsanov, S.S., Derbeneva, S.S., and Shestakova, N.A. (1966) Optical width of the forbidden band. Tin halides and chalcohalides. Izvestiya Akademii Nauk SSSR, Neorganicheskie Materialy, 2, 2251 (in Russian).

Bernard, A.A. and Le Guern, F. (1986) Condensation of volatile elements in high-temperature gases of Mount St. Helens. Journal of Volcanology and Geothermal Research, 28, 91–105.

Borodaev, Yu.S., Garavelli, A., Garbarino, C., Grillo, S.M., Mozgova, N.N., Uspenskaya, T.Yu., and Vurro, F. (2001) Rare sulfosalts from Vulcano, Aeolian Islands, Italy. IV. Lillianite. Canadian Mineralogist, 39, 1383–1396.

Borodaev, Yu.S., Garavelli, A., Garbarino, C., Grillo, S.M., Mozgova, N.N., Paar, W.H., Topa, D., and Vurro, F. (2003) Rare sulfosalts from Vulcano, Aeolian Islands, Italy. V. Selenian heyrovskýite. Canadian Mineralogist, 41, 429–440.

Brese, N.E. and O'Keeffe, M. (1991) Bond-valence parameters for solids. Acta Crystallographica, B47, 192–197.

Breskovska, V.V., Mozgova, N.N., Bortnikov, N.S., Gorshov, A.I., and Tsepin, A.I. (1982) Ardaite—a new lead antimony chlorosulphosalt. Mineralogical Magazine, 46, 357–361.

Chaplygin, I.V., Mozgova, N.N., Magazina, L.O., Kuznetsova, O.Yu., Safonov, Yu.G., Bryzgalov, I.A., Makovicky, E., and Balić-Žunić, T. (2005) Kudriavite, $(Cd,Pb)Bi_2S_4$, a new mineral species from Kudriavy volcano, Iturup Island, Kurile arc, Russia. Canadian Mineralogist, 43, 695–701.

Cheynet, B., Dall'Aglio, M., Garavelli, A., Grasso, M.F., and Vurro, F. (2000) Trace elements from fumaroles at Vulcano Island (Italy): Rates of transport and a thermochemical model. Journal of Volcanology and Geothermal Research, 95, 273–283.

Demartin, F., Gramaccioli, C.M., Campostrini, I., and Orlandi, P. (2008) Demicheleite, BiSBr, a new mineral from La Fossa crater, Vulcano, Aeolian Islands, Italy. American Mineralogist, 93, 1603–1607.

Doussier, C., Moëlo, Y., Léone, P., and Meerschaut, A. (2007) $(Mn_{1-x}Pb_x)Pb_{10+y}Sb_{12-y}S_{26-y}Cl_{4+y}O$, a new oxy-chloro-sulfide with ≈ 2 nm-spaced (Mn,Pb)Cl$_4$ single chains within a waffle-type crystal structure. Journal of Solid State Chemistry, 180, 2323–2334.

Doussier, C., Moëlo, Y., Meerschaut, A., Léone, P., and Guillot-Deudon, C. (2008) Crystal structure of the new compound $Pb_{3+x}Sb_{3-x}S_{7-x}Cl_{1+x}$(x~0.45): The homologous series $Pb_{(2+2N)}(Sb,Pb)_{(2+2N)}S_{(2+2N)}(S,Cl)_{(4+2N)}Cl_N$ and its polychalcogenide derivatives (N=1–3). Journal of Solid State Chemistry, 181, 920–934.

Downs, R.T., Bartelmehs, K.L., Gibbs, G.V., and Boisen Jr., M.B. (1993) Interactive software for calculating and displaying X-ray or neutron powder diffractometer patterns of crystalline materials. American Mineralogist, 78, 1104–1107.

Fenner, J. (1978) Die Kristallstruktur des Zinnsulfidiodids Sn_4SI_6. Zeitschrift fuer Naturforschung, Teil B. Anorganische Chemie, Organische Chemie, 33, 479–481.

Garavelli, A. (1994) Mineralogia e geochimica di fasi vulcaniche condensate: i sublimati dell'isola di Vulcano tra il 1990 ed il 1993, 171 p. Ph.D. thesis, Università di Bari, Italy.

Garavelli, A., Laviano, R., and Vurro, F. (1997) Sublimate deposition from hydrothermal fluids at the Fossa crater, Vulcano, Italy. European Journal of Mineralogy, 9, 423–432.

Garavelli, A., Mozgova, N.N., Orlandi, P., Bonaccorsi, E., Pinto, D., Moëlo, Y., and Borodaev, Yu. (2005) Rare sulfosalts from Vulcano, Aeolian Islands, Italy. VI. Vurroite, $Pb_{20}Sn_2(Bi,As)_{22}S_{54}Cl_6$, a new mineral species. Canadian Mineralogist, 43, 703–711.

Gaudin, E., Petříček, V., Boucher, F., Taulelle, F., and Evain, M. (2000) Structures and phase transitions of the A_7PSe_6 (A = Ag, Cu) argyrodite-type ionic conductors. III. α-Cu_7PSe_6. Acta Crystallographica, B56, 972–979.

Makovicky, E. and Balić-Žunić, T. (1998) New measure of distortion for coordination polyhedra. Acta Crystallographica, B54, 766–773.

Makovicky, E., Topa, D., and Mumme, W.G. (2006) The crystal structure of dadsonite. Canadian Mineralogist, 44, 1499–1512.

Meerschaut, A., Palvadeau, P., Moëlo, Y., and Orlandi, P. (2001) Lead-antimony sulfosalts from Tuscany (Italy). IV. Crystal structure of pillaite, $Pb_9Sb_{10}S_{23}ClO_{0.5}$, an expanded monoclinic derivative of hexagonal $Bi(Bi_2S_3)_9I_3$, from the zinkenite group. European Journal of Mineralogy, 13, 779–790.

Miehe, G. and Kupčík, V. (1971) Die Kristallstruktur des $Bi(Bi_2S_3)_9J_3$. Naturwissenschaften, 58, 219–220.

Moëlo, Y. (1979) Quaternary compounds in the system Pb-Sb-S-Cl: Dadsonite and synthetic phases. Canadian Mineralogist, 17, 595–600.

Moëlo, Y., Makovicky, E., and Karup-Møller, S. (1984) New data on the minerals of the andorite series. Neues Jahrbuch für Mineralogie Monatshefte, 4,

175–182.

——— (1989) Sulfures complexes plombo-argentifères: minéralogie et cristallochimie de la série andorite-fizélyite, $(Pb,Mn,Fe,Cd,Sn)_{3-2x}(Ag,Cu)_x$ $(Sb,Bi,As)_{2+x}(S,Se)_6$. Documents du BRGM, 167, BRGM Edit. (Orléans), 107 p.

Muranatsu, Y. and Wedepohl K.H. (1998) The distribution of iodine in the Earth's crust. Chemical Geology, 147, 201–216.

Nespolo, M. and Ferraris, G. (2001) Effects of the stacking faults on the calculated electron density of mica polytypes—The Ďurovič effect. European Journal of Mineralogy, 13, 1035–1045.

Orlandi, P., Moëlo, Y., Meerschaut, A., and Palvadeau, P. (2001) Lead–antimony sulfosalts from Tuscany (Italy). III. Pillaite, $Pb_9Sb_{10}S_{23}ClO_{0.5}$, a new Pb-Sb oxy-chloro-sulfosalt, from Buca della Vena mine. European Journal of Mineralogy, 13, 605–610.

Orlandi, P., Moëlo, Y., Meerschaut, A., Palvadeau, P., and Léone, P. (2004) Lead-antimony sulfosalts from Tuscany (Italy). VI. Pellouxite, $(Cu,Ag)_2Pb_{21}Sb_{23}S_{55}ClO$, a new oxy-chlorosulfosalt from Buca della Vena mine, Apuan Alps. European Journal of Mineralogy, 16, 839–844.

Otwinowsky, Z. and Minor, W. (1997) Processing of X-ray diffraction data collected in oscillation mode. Methods in Enzymology, 276, 307–326.

Pattrick, R.A.D. (1978) Microprobe analyses of cadmium-rich tetrahedrites from Tyndrum, Perthshire, Scotland. Mineralogical Magazine, 42, 286–288.

Pauling, L. (1960) The Nature of Chemical Bond and the Structure of Molecules and Crystals: An Introduction to Modern Structural Chemistry, 3rd edition, 664 p. Cornell University Press, New York.

Petříček, V., Dušek, M., and Palatinus, L. (2000) JANA2000, a crystallographic computing system. Institute of Physics, Academy of Sciences of the Czech Republic, Prague.

Pinto, D. (2004) Mineralogy, crystal chemistry and structures of sulfosalts from Vulcano (Aeolian Islands, Italy): Ag-free lillianite, Cl-bearing galenobismutite, kirkiite, and the new mineral vurroite, 165 p. Ph.D. thesis, Università di Bari, Italy.

Pinto, D., Bonaccorsi, E., Balić-Žunić, T., and Makovicky, E. (2008) The crystal structure of vurroite, $Pb_{20}Sn_2(Bi,As)_{22}S_{54}Cl_6$: OD-character, polytypism, twinning, and modular description. American Mineralogist, 93, 713–727.

Pinto, D., Balić-Žunić, T., Bonaccorsi, E., Borodaev, Yu., Garavelli, A., Garbarino, C., Makovicky, E., Mozgova, N.N., and Vurro, F. (2006) Rare sulfosalts from Vulcano, Aeolian Islands, Italy. VII. Cl-bearing galenobismutite. Canadian Mineralogist, 44, 443–457.

Quisefit, J.P., Toutain, J.P., Bergametti, G., Javoy, M., Cheynet, B., and Person, A. (1989) Evolution versus cooling of gaseous volcanic emissions from Momotombo Volcano, Nicaragua: Thermochemical model and observations. Geochimica et Cosmochimica Acta, 53, 2591–2608.

Roberts, A.C., Venance, K.E., Seward, T.M., Grice, J.D., and Paar, W.H. (2006) Lafossaite, a new mineral from the La Fossa crater, Vulcano, Italy. The Min-

eralogical Record, 37, 165–168.

Rolies, M.M. and de Ranter, C.J. (1978) A new investigation of ammonium cadmium chloride. Acta Crystallographica, B34, 3057–3059.

Sheldrick, G.M. (1997) SHELXL-97. A program for crystal structure refinement. University of Göttingen, Germany.

Symonds, R.B. (1993) Scanning electron microscope observations of sublimates from Merapi Volcano, Indonesia. Geochemical Journal, 26, 337–350.

Symonds, R.B. and Reed, M.H. (1993) Calculation of multicomponent chemical equilibria in gas-solid-liquid systems: calculation methods, thermochemical data and applications to studies of high-temperature volcanic gases with examples from Mount St. Helens. American Journal of Science, 293, 758–864.

Symonds, R.B., Rose, W.I., Reed, M.H., Lichte, F.E., and Finnegan, D.L. (1987) Volatilization, transport, and sublimation of metallic and non-metallic elements in high-temperature gases at Merapi Volcano, Indonesia. Geochimica et Cosmochimica Acta, 51, 2083–2101.

Symonds, R.B., Reed, M.H., and Rose, W.I. (1992) Origin, speciation, and fluxes of trace element gases at Augustine volcano, Alaska: Insights into magma degassing and fumarolic processes. Geochimica et Cosmochimica Acta, 56, 633–657.

Thévet, F., Nguyen, H.D., Dagron, C., and Flahaut, J. (1976) Contribution à l'étude du système formé par l'étain, le soufre et l'iode. Mise en évidence des deux variétés de l'iodosulfure stanneux Sn_2SI_2: Comportement thermique et étude structurale. Journal of Solid State Chemistry, 18, 175–182.

Voutsas, G.P. and Rentzeperis, P.J. (1980) The crystal structure of the paraelectric bismuth thiochloride BiSCl. Zeitschrift für Kristallographie, 152, 109–118.

Vurro, F., Garavelli, A., Garbarino, C., Moëlo, Y., and Borodaev, Yu. (1999) Rare sulfosalts from Vulcano, Aeolian Islands, Italy. II. Mozgovaite, $PbBi_4(S,Se)_7$, a new mineral species. Canadian Mineralogist, 37, 1499–1506.

Zelenski, M.E. (2003) Transport of elements and mineral forming conditions at high-temperature gas discharges from Mutnovsky volcano (Kamchatka), 121 p. Ph.D. thesis, Institute of Vulcanology, Petropavlovsk-Kamchatsky.

Zelenski, M. and Bortnikova, S. (2005) Sublimate speciation at Mutnovsky volcano, Kamchatka. European Journal of Mineralogy, 17, 107–118.

Zelenski, M., Balić-Žunić, T., Bindi, L., Garavelli, A., Makovicky, E., Pinto, D., and Vurro, F. (2006) First occurrence of iodine in natural sulfosalts: The case of mutnovskite, $Pb_2AsS_3(I,Cl,Br)$, a new mineral from the Mutnovsky volcano, Kamchatka Peninsula, Russian Federation. American Mineralogist, 91, 21–28.